FRACTURE QUANTIFICATION AND MODELING IN THE TENSLEEP SANDSTONE NEAR THE ALKALI FAULT, BIGHORN BASIN, WYOMING

by

Alper T. Kilic

A thesis submitted to the Faculty and Board of Trustees of Colorado School of Mines in partial fulfillment of the requirements for the degree of Master of Science (Geology).

Golden, Colorado

Date_____

Signed:_____
Alper T. Kilic

Signed:_____
Neil F. Hurley

Golden, Colorado

Date_____

_____
Dr. Murray Hitzman
Professor and Head,
Department of Geology
and Geological Engineering

ABSTRACT

This thesis documents fractures exposed in outcrop along the Alkali fault in the Bighorn basin, Wyoming. The Alkali fault is a major east-west trending oblique-slip fault that cuts the Tensleep Sandstone, which is an important hydrocarbon producer in the area. These fractures are mainly deformation bands (gouge-filled fractures), and conjugate shear fractures that are filled with calcite. The highest fracture intensity occurs near the fault.

Fracture analysis has been done by taking 20 scanline surveys at various distances, roughly perpendicular and parallel to the fault. Scanline surveys permit orientation of fracture sets and quantification of fracture spacing. Other basic fracture information was collected, such as filling and length of the fractures, and sense of offset along the fractures.

The Alkali fault and locations of the scan-line surveys were determined utilizing GPS (Global Positioning System). After these scan-line surveys were interpreted, a fracture model of the study area was built. Compartment areas were calculated as a function of distance from the Alkali fault.

Six fracture sets are detected in the study area. Sets 1, 2, 3, and 4 are controlled by the Alkali fault and spacing increases with distance from the fault. Fracture spacing increases from 0.5-11 ft (0.15-3.3 m) for Set 1, 0.5-8 ft (0.15-2.4 m) for Set 2, 0.5-8 ft (0.15-2.4 m) for Set 3, and 2-9 ft (0.6-2.7 m) for Set 4. Fracture Sets 5 and 6, which are open fractures, appear to be regional fracture sets of the Bighorn basin.

The Alkali fault has a roughly east-west strike azimuth. Fracture set 1 is oriented 226/80˚, fracture set 2 is oriented 251/84˚, fracture set 3 is oriented 205/87˚, and fracture set 4 is oriented 273/88˚. None of these fracture sets are consistent with a primarily dip-slip sense of offset on the Alkali fault. Lateral sense of offset is inferred for Alkali fault movement that gave rise to the main fracture sets.

Healed fractures cause compartmentalization in the study area. Compartments are bounded by healed fractures that should act as permeability barriers. Size of the compartments ranges from 1 to 20 ft^2 (0.1-1.9 m^2) near the fault, up to 10,000 ft^2 (929 m^2) at 1,000 ft (305 m) distance from the fault.

TABLE OF CONTENTS

Page

Page

Page

LIST OF FIGURES

Page

Page

Page

Page

LIST OF FIGURES

Page

Page

Page

Page

LIST OF TABLES

Page

ACKNOWLEDGMENTS

I am greatly indebted to the Republic of Turkey and the Turkish Petroleum Corporation for providing me financial support, which made it possible for me to study at the Colorado School of Mines.

I would like to express gratitude to my advisor, Dr. Neil Hurley, for his guidance, suggestions, and generous contribution of his time. Sincere appreciation is also expressed to Dr. John Curtis, Dr. Mary Carr, and Dr. Tom Davis for being great professors and committee members.

I also wish to express my appreciation to Dr. David Richards, Dr. Paul Griffiths and Dr. Stephen Calvert for both helping and teaching me how to use 3DMove structural analysis software.

I would like to thank Dr. Ozcan Yigit for discussing problems related to my thesis. I also thank Bozkurt N. Ciftci and Dr. Alex Aviantara for being my companions during the field work.

Chapter 1

INTRODUCTION

The Tensleep Sandstone is a Middle Pennsylvanian to Lower Permian-aged eolian sandstone with interbedded carbonates. The Tensleep Sandstone is an important hydrocarbon producer in the Rocky Mountains. Production from the Tensleep Sandstone began during the 1920's and 30's. Fluctuations in the oil price caused production to vary from the 1920's to the 1970's. The Tensleep Sandstone has been thought of as a relatively homogeneous sand body lacking any kind of important heterogeneities in many previous reservoir models. Consequently, low recoveries and inefficient EOR operations occurred during most of the production history, leaving behind significant remaining potential. Recent studies suggest that compartmentalization occurs because of eolian dune bodies, faults and fractures.

Fracturing in Tensleep reservoirs, in general, has a negative effect on hydrocarbon production. Closely spaced fractures can impede horizontal fluid flow. Low permeability normal to the fractures disrupts radial flow and creates directional permeability. Also, vertical open fractures cause high water cut even though high oil saturations may be detected from core analysis.

This thesis focuses on fractures along the Alkali fault in the Bighorn basin, Wyoming (Figure 1.1). The Alkali fault is major east-west trending oblique-slip fault that cuts the Tensleep Sandstone. Fractures in the Tensleep Sandstone associated with this fault are mainly deformation bands that are filled with cement and mylonite. Fracture intensity is very high near the fault. There is a very distinctive fault scarp in the Alkali Creek study area on the southwest flank of the Bighorn Mountains.

This study quantifies spacing and orientation of healed and open fractures in the Tensleep Sandstone near the Alkali fault. This information will improve our understanding of production from such reservoirs.

1.1 Research Objectives

A main purpose of this thesis was to see the effects of the fracture system on fluid flow. Another goal was to combine fracture data with depositional bounding surfaces to discuss the effectiveness of drilling a well near a fault in eolian sandstone. The specific objectives are:

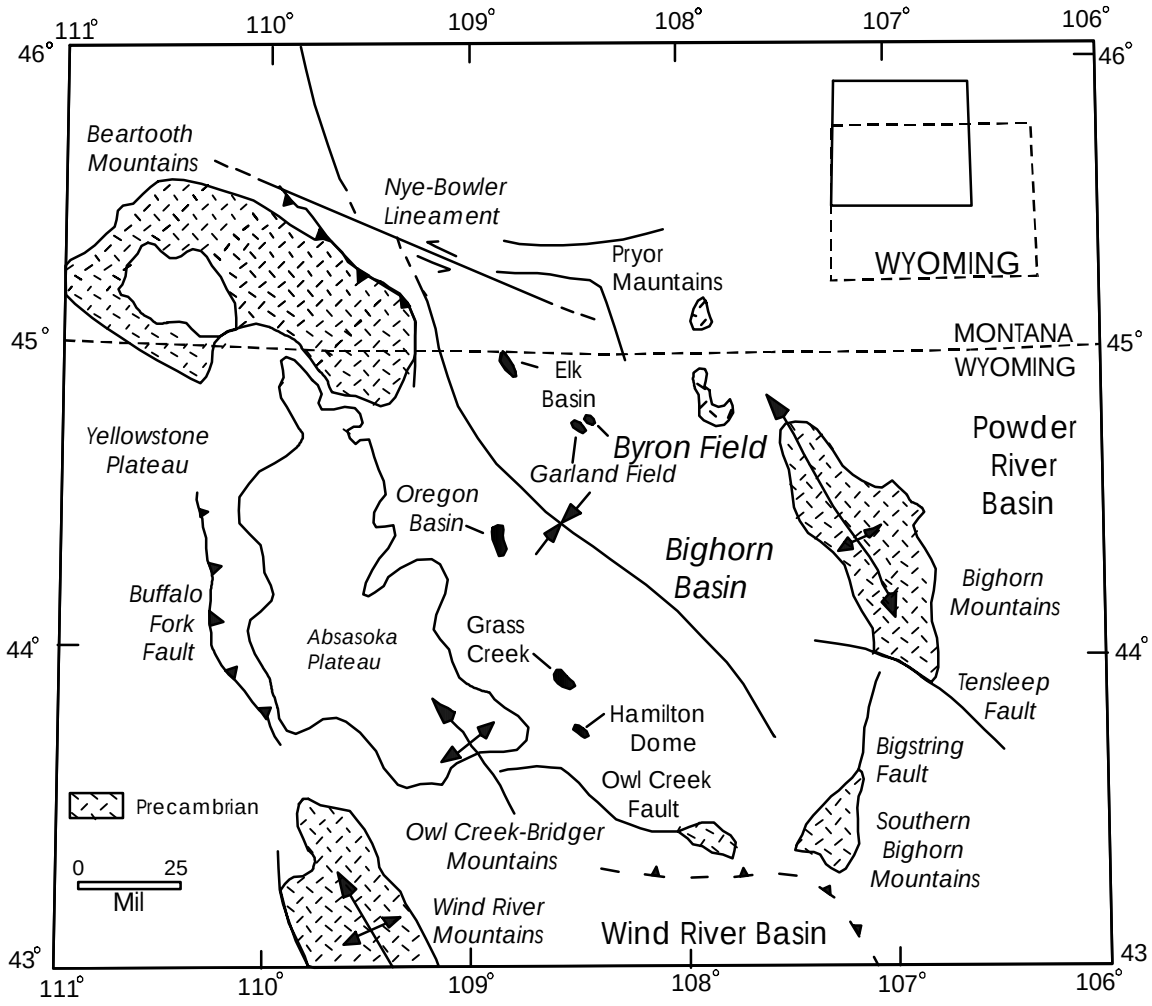

Figure 1.1 Oil fields, basement uplifts, and structural features of the Bighorn basin. From Hurley et al. (2000).

1- Detect fracture spacing relative to distance from the Alkali fault.

2- Characterize the geometry of the fracture network.

3- Determine compartment size as a function of distance from the Alkali fault.

4- Discuss the application of these results to other fractured reservoirs.

1.2 Previous Work

The Middle Pennsylvanian and Lower Permian Tensleep Sandstone has been producing large quantities of petroleum since the beginning of the 20th century. This is one of the earliest reservoirs exploited in the state of Wyoming. For this reason, the Tensleep Sandstone and its stratigraphic equivalents are important to geologists. Geologists (Agatston, 1954; Keefer and Van Lieu, 1966; Emmett et al., 1971; Sando et al., 1975) who worked before the mid-1970's claimed that the Tensleep Sandstone was deposited in a shallow marine environment as a homogenous body without significant permeability barriers. Studies in recent years have shown that the Tensleep Sandstone was deposited as an eolian and marine sandstone (Fox et al., 1975; Shebl, 1995a, 1995b; Carr-Crabaugh and Dunn, 1996; Iverson et al., 1996; Aviantara, 1999).

The Tensleep Sandstone was defined by Darton (1904) as a thick sandstone at the type locality at Tensleep Canyon, Washakie County, Wyoming. Agatston (1954) worked in detail on the Tensleep Sandstone on the west flank of the northern Bighorn basin. He described the Tensleep Sandstone as a cross-bedded, massive sandstone with dolomite,

limestone and some shale and anhydrite beds. He observed that the lower part was more dolomitic than the upper part. Also, he compared the carbonate rock ratio and concluded that thin beds of limestone thickened towards the main area of carbonate deposition in eastern Wyoming.

Keefer and van Lieu (1966) worked in detail on the Tensleep Sandstone in the Wind River basin. They pointed out that the Tensleep Sandstone is predominantly cross-bedded sandstone. Interbeds of chert occur at the base. Thin dolomite and carbonate strata occur throughout the Tensleep, and are especially common in the basal part. Their interpretation of the depositional environment was that sandstone vs. carbonate deposition occurred as a result of advancing and retreating of the sea.

Fox et al. (1975) worked on porosity variability within the Tensleep Sandstone in the Bighorn, Wind River, and Green River basins of Wyoming. They concluded that porosity generally decreased with increasing depth of burial. Permeability decreased as porosity decreased. Their study revealed that increasing depth caused overgrowth of orthochemical quartz around detrital quartz which filled pore spaces.

Most studies after 1975 have focused on lithological descriptions, facies correlation, and petrophysical features such as porosity, permeability and fractures. The goal is to improve hydrocarbon recovery. These studies were done in the producing areas in the Bighorn basin and adjacent basins on equivalent units such as the Weber, Quadrant, Casper, and Minnelusa Formations (Emmet et al., 1971; Shebl, 1995a, 1995b; Carr-Crabaugh and Dunn, 1996; Iverson et al., 1996; Aviantara, 1999).

Emmett et al. (1971) studied the Little Buffalo Basin field, which is on the southwest side of the Bighorn basin. They reached the conclusion that the dolomite layers within the Tensleep Sandstone cannot be correlated from well to well. Some of these dolomitic layers grade laterally into sandstone. These layers are almost impermeable. They do not allow communication between sand bodies. Core studies showed that in some areas of the reservoir, especially near the anticline axis where maximum flexure occurred, there are many vertical fractures. Dolomitic layers between sand zones are not effective barriers in areas where such fractures exist.

Morgan et al. (1978) researched the Tensleep Sandstone in the Oregon Basin field, which is located on the west side of the Bighorn basin. The field is about 9 mi (15km) long and is composed of a north dome and a south dome. They interpreted the depositional environment as marine and partly eolian, whereas it was previously interpreted as a shallow marine and marine environment. Also they believed that a combination of original depositional characteristics and post-depositional cementation caused the Tensleep to be a highly layered reservoir. In Oregon Basin field, the Tensleep Sandstone is about 200 ft (60m) thick but locally this thickness decreases to 60 ft (18m). Reservoir thickness changes occur as a result of post-Tensleep erosion. They dealt with the issue of reservoir variations in the Tensleep Sandstone. In addition, they observed three kinds of cement: anhydrite, dolomite, and quartz. The presence of anhydrite and dolomite cements caused the Tensleep Sandstone to be locally of non-reservoir quality. Two fracture sets were observed in Oregon Basin, both at the surface and in the Tensleep.

These are closed fractures that were more concentrated in the crestal areas than on the edges of the dome. These are roughly oriented north–south and east-west. Fractures in the Oregon Basin field were interpreted as local anomalies that did not have a dominant role in field-wide performance.

Mankiewicz and Steidtmann (1979) worked on Tensleep Sandstone depositional environment and diagenesis in the eastern Bighorn basin. They compared the Tensleep Sandstone depositional environment to the present-day Qatar peninsula, in which barchanoid dune complexes migrate into the sea over Eocene dolomite. They believed that the Tensleep Sandstone in the Bighorn basin was deposited in a coastal environment. The lower Tensleep Sandstone, approximately 60 ft (18 m) thick, was deposited under primarily supratidal, intertidal, subtidal, and lagoonal conditions. Eolian dune sands, with cross strata being of relatively small scale, are generally thinner than 6 ft (2 m). The upper Tensleep represents a depositional environment that is dominantly eolian with associated sands that formed in sabkha environments. The eolian dune sands occur in laterally continuous sets up to 30 ft (10m) thick. Sands are finely laminated with large-scale trough and planar tabular cross stratification with dip angles between 15-31°. Also, they pointed out that the Tensleep Sandstone has early diagenesis which occurred just after deposition. Gypsum and dolomite cementation took place by means of recharge water at the sabkha surface. Later cementation caused calcite and dolomite precipitation as a result of changes in basin hydrology during regional downwarping during the Jurassic.

Vealey (1991) suggested that the upper Tensleep in the Wind River basin was deposited entirely in an eolian depositional environment. He claimed that no marine sediments were seen in the upper Tensleep. He identified dolomites in the area as deposits that were the result of water table fluctuations.

South Casper Creek field, which is an oil producer in the Tensleep, is a heavily studied area for reservoir characterization. Tanean (1991) found fracturing and faulting using well logs and seismic sections. Formation MicroScanner logs (Schlumberger) show that fractures within the Tensleep predominantly occur in dolomite zones. These zones are generally marine in origin, such as burrowed sandstones or interdune deposits. Six FMS (Formation MicroScanner) logs show trends mostly parallel to major faults in the south dome.

Aviantara (1999) differentiated the hierarchy of Tensleep architectural elements. These are: eolian stratification, eolian surface-bounded elements, facies, parasequences, and system tracts in the Tensleep Sandstone. This work was based on an outcrop study at Alkali Creek, Ziesman Dome, and Cold Spring Road and subsurface studies at Byron and Bonanza fields in the Bighorn basin. He showed that the progradation of the eolian dunes was in a south-southwest direction. First-order bounding surfaces climb at a 0.9 to 2.9° angle, generally parallel to foreset dip direction, which is to the south-southwest. He detected two sets of open fractures by interpreting pseudo-images and borehole images from both horizontal and verticals wells at Byron field. Fracture strike azimuth is roughly

perpendicular to each other and the main fracture orientation occurs in a northeast-southwest direction.

Ciftci (2001) studied Alkali Creek, which is the study area of this thesis. He showed in his thesis the geometry and volumetric size of compartments in the Tensleep Sandstone using Earth Vision (Dynamic Graphics) software, based on data collected from outcrop exposures. He used more than 3500 data points to delineate first- and second-order surfaces and compartments that occurred as a result of bounding surfaces in the Tensleep. He concluded that first-order bounded compartments are laterally extensive and display variable thickness in the range of 6 to 80 ft (2 to 26m). Compartments subdivided by second-order bounding surfaces have an average spacing of 100 ft (30 m) and display variations in their strike orientation to form laterally discontinuous bounded compartments. After simulating the wells by using 10-acre, 40-acre, 80-acre, and 160-acre templates in the 3-D model, he pointed out that horizontal wells drilled parallel to foreset dip direction drain the maximum number and volume of reservoir compartments.

Hurley et al. (2000) used core, outcrop studies, and log correlation to define facies architecture at Byron field (Figure 1.1). They observed two orthogonal open fracture sets whose strikes and dips are N49W / 88SW (Set1) and N43E / 69NW (Set2). The mean spacing of the Set 1 fractures is about 7.5 ft (2.3 m). For Set 2 fractures, mean spacing is 3.0 ft (0.9 m).

1.3 Research Contributions

GPS provides an accurate way to position faults and scanline locations on a map. By using GPS, the Alkali fault orientation is approximately N85E.

Six main fracture sets are detected in the study area after plotting fracture strikes and dips on contoured stereonets. Sets 1, 2, 3, 4 are the controlled by the Alkali fault. Spacing gets larger when going away from the fault. Fracture spacing increases from 0.5-11 ft (0.15-3.3 m) for Set 1, 0.5-8 ft (0.15-2.4 m) for Set 2, 0.5-8 ft (0.15-2.4 m) for Set 3 and 2-9 ft (0.6-2.7 m) for Set 4. Fracture set 4 is developed as deformation bands near the fault. Fracture sets 5 and 6 are regional fracture sets of the Bighorn basin. Regional fractures are open fractures. This suggests that they occurred after regional diagenesis.

Fracture set 1 is oriented 46/80, fracture set 2 is oriented 71/84, fracture set 3 is oriented 25/87, fracture set 4 is oriented 2/87. Fracture direction plays a significant role to determine principle stresses of the area. Fracture set 1 is the same direction as the maximum principle stress. Fracture sets 2 and 3 took place depending on the maximum stress direction as conjugate fracture sets.

Size of the compartments is 1 to 30 ft^2 (0.1- 2.8 m^2) near the fault. The compartment sizes get to 10,000 ft^2 (929 m^2) at 1000 ft (305 m) distance from the fault. Drilling near an oblique-slip fault is not a good idea in a Tensleep reservoir. Fault movement causes shear fractures and deformation bands to form near the fault. These fractures and deformation bands create permeability barriers and small compartments in the reservoirs.

Chapter 2

GEOLOGICAL SETTING

2.1 Location of Study Area

Exposures of the Tensleep Sandstone occur in the Bighorn basin of north-central Wyoming (Figure 2.1). The study area covers approximately 2000 acres (8 km^2) at Alkali Creek where the Tensleep Sandstone is well exposed. The Alkali fault, which is approximately 6 mi (10 km) long, consists of dip-slip and strike-slip faults which have an east-west orientation on the eastern side of the Bighorn basin. One of the main reasons for choosing Alkali Creek is that there is a very distinctive fault scarp. Also, the area is suitable for outcrop studies because of the orientation and lateral extent of cliff faces and spacing of the canyon exposures (Figure 2.2). In addition, the research that was done approximately in the same area by Ciftci (2001) provided us data availability.

The study area lies in Sections 29 and 30 of T51N- R89W, located approximately 30 mi (48 km) north of Tensleep and 32 mi (51 km) southeast of Greybull (Figure 2.1). All scanline surveys were investigated in the south part of the fault scarp where NE-SW oriented canyons lie roughly perpendicular to the foreset direction. These canyons are parallel to one of main fracture systems in the study area.

Figure 2.1

Figure 2.2

2.2 Stratigraphy

2.2.1 Regional Stratigraphy

The Tensleep Sandstone consists of Middle Pennsylvanian (Demoinesian) to Lower Permian (Wolfcampian) shallow marine and eolian deposits. The age is mainly based on fusulinids, brachiopods, and conodonts studied by Henbest (1956), Verville (1957), Hoare and Burgess, (1960), and Rhodes (1963). *Schwagerina* and *Triticites* fusulinids, which are shallow marine fossils, are common in the Tensleep Sandstone (Verville, 1957; Burgess, 1961). The unit is variable in thickness as a result of differential erosion across the top of the Tensleep Sandstone (Kerr, 1989; Kerr et al., 1986; Wheeler, 1986). Eolian deposits in the Tensleep were described as fine to very fine grained, well-rounded, well-sorted quartz arenites by Aviantara (2000).

The Tensleep Sandstone lies conformably above the red beds and cherty carbonates of the Amsden Formation (Figure 2.3). The Phosphoria Formation, which is represented by the Goose Egg Formation in the study area (Figure 2.3), includes red beds, shales, evaporites and dolomites. The Goose Egg unconformably overlies the Tensleep Sandstone. The Tensleep Sandstone was deposited in a highstand systems tract, whereas the Amsden Formation was deposited in a transgressive systems tract (Kerr, 1989). The upper, Absaroka II, sequence (Figure 2.3) , which starts with incised valley

Figure 2.3

fills of the Goose Egg Formation, was deposited on the eroded surface of the Tensleep Sandstone.

The lower, Absaroka I, sequence (Figure 2.3), which starts with incised valley fills of the Darwin Sandstone member of the Amsden Formation, was deposited on the eroded surface of the Mississippian Madison Limestone.

Outcrop and subsurface studies demonstrate that the Tensleep Sandstone includes a number of parasequences, which consist of dolomitic sandstone, marine sandstone, and eolian sandstone (Kerr, 1989). These parasequences occur as a result of changes in sea level. The dolomitic sandstones represent sea-level rise, and eolian sandstones are the result of sea-level fall (Kerr et al., 1986; Kerr and Dott, 1988; Kerr, 1989).

Studies in recent years have shown that the Tensleep Sandstone was deposited in both an eolian and marine environment (Morgan et al., 1978; Desmond et al., 1984; Kerr et al., 1986; Wheeler, 1986; Rittersbacher, 1985; Kerr and Dott, 1988; Kerr, 1988; Carr-Crabaugh and Dunn, 1996).

The eolian sandstones in the Tensleep consist of fine to very fine grained, rounded, well sorted quartz arenites. Dunes along the west flank of the Bighorn Mountains are oblique , slightly sinuous crested features that supported smaller crescentic dunes (Kerr and Dott, 1988). Paleocurrent studies show that dunes migrated to the south and southwest where the shoreline was located (Mankiewicz and Steidtmann, 1979; Kerr and Dott, 1988).

2.2.2 Local Stratigraphy

2.2.2.1 Tensleep Sandstone

The Tensleep Sandstone was named at the type locality in the Tensleep Canyon by Darton (1904). He divided the strata overlying the Mississippian Madison Limestone and underlying the Permian Goose Egg Formation into the Amsden Formation and the Tensleep Sandstone.

The Tensleep Sandstone was deposited on a broad coastal plain during the middle Pennsylvanian and Lower Permian in both eolian and marine environments (Kerr and Dott, 1988; Carr-Crabaugh and Dunn, 1996). Outcrop and subsurface studies showed that the Tensleep Sandstone includes repetitive parasequences of dolomitic sandstone, marine sandstone and cross-bedded, quartz-rich, eolian sandstone (Kerr, 1989; Aviantara, 2000).

The Tensleep conformably overlies the Amsden Formation. The contact occurs where subtidal and lagoonal dolostones of the Amsden Formation interfinger with intertidal and supratidal sandy dolostones, and anhydrite of the lower Tensleep Sandstone (Andrews and Higgins, 1984). The Goose Egg unconformably overlies the Tensleep. The Amsden Formation, the product of transgressive system tract deposits, unconformably covers the Madison Formation. Tensleep parasequences occurred as a result of sea-level fluctuations during which the dolomitic sandstones show sea level rise, and eolian

sandstones represent sea-level fall (Figure 2.4) (Kerr et al., 1989; Kerr and Dott, 1988; Kerr, 1989).

The Tensleep Sandstone is divided into two parts by recent studies. The lower unit (Figure 2.5) consists of supratidal, intertidal, and subtidal to lagoonal sediments with a high proportion of chemical to clastic rock and rarely, small-scale eolian cross strata (Andrews and Higgins., 1984). The upper unit (Figure 2.5) consists of large-scale eolian cross strata and associated interdunal sabkha deposits (Andrews and Higgins., 1984). The upper unit is mainly clastic constituents, which provides better reservoir rock. The eolian portion of the Tensleep Sandstone consists of very fine to fine grained, rounded, well-sorted quartz arenites. The sedimentary structures in the Tensleep Sandstone range from well-formed trough to planar tabular cross-stratification with dip angles between 10-30° (Andrews and Higgins, 1984).

The Tensleep Sandstone varies in thickness. These thickness variations are explained by many authors as a combination of post-Tensleep erosion and original depositional patterns (Kerr et al., 1989; Kerr and Dott, 1988).

Bounding surfaces, which are first (1.0), second (2.0), and third (3.0) order surfaces, divide the Tensleep Sandstone into compartments. It has been observed that bounding surfaces are very good permeability barriers which affect oil movement

Figure 2.4

Figure 2.5

negatively. In both horizontal and vertical directions, 1.0-bounding surfaces separate large-scale tabular-planar eolian cross-stratified sets (Figure 2.6) (Kerr and Dott, 1988; Aviantara, 2000). In each of these sets, cross stratification is tangential to an underlying 1.0-bounding surface at the bottom and is truncated by the overlying 1.0-bounding surfaces. 2.0 bounding surfaces lie between first order surfaces and separate bundles of eolian cross-strata sets (Figure 2.7)(Kerr and Dott, 1988). 3.0-bounding surfaces (Brookfield, 1977) are reactivation surfaces that bound eolian cross-strata sets.

2.2.2.2 Petrography and Diagenesis

A study done by Akhtar (1991) in South Casper Creek oil field showed that the Tensleep Sandstone is fine to very fine grained, with average grain size ranging from 0.9 mm (3.5 phi) to 0.25 mm (1.5 phi) (Figure 2.8). Sands are moderately well sorted to well sorted with standard deviation ranging from 0.35 to 0.74 phi units (Akhtar, 1991). Part of the Tensleep Sandstone has poor sorting based on alternating, parallel, very fine grained wind ripple laminae and fine to medium grained grainfall laminae. Each individual lamina is very well sorted but too thin to account for the whole sample. Grains in grainflow laminae are subrounded to rounded whereas they are sub-angular in the wind ripple laminae.

Figure 2.6

Figure 2.8

The Tensleep Sandstone consists of 79-99% quartz, with the remainder being potassium feldspar (Akhtar, 1991) (Figure 2.9). Also, grains of zircon, tourmaline and rutile are present as heavy minerals. This extremely mature texture and mineralogy is a function of transport distance. Todd (1964) postulated that the Canadian Shield and the overlying sedimentary rocks provided the provenance for the Tensleep Sandstone. The high textural maturity and predominant south-southwest paleocurrent direction (Opdyke and Runcorn, 1960) led him to this interpretation.

Various kinds of diagenetic cement were found in the Tensleep Sandstone. The most common cements are silica, anhydrite and calcite.

Feldspar and kaolinite cements are also present (Mankiewicz and Steidtmann, 1979). Silica occurs as quartz overgrowths on detrital grains, as cherty nodules in dolomites and sandy dolomites, and as chalcedony in radial fibrous form (Mankiewicz and Steidtmann, 1979). Anhydrite is a conspicuous sandstone cement in the subsurface, whereas it is replaced by calcium carbonate at the surface. Anhydrite is locally present at the surface where algal mat and intertidal dolomites occur (Mankiewicz and Steidtmann,

Figure 2.9

1979). Calcite occurrence in surface rocks is generally in vug and burrow and fracture fillings. The presence of calcite as a cement in surface exposures suggests that this is the most recent cementing event.

Mankiewicz and Steidtmann (1979) suggested that early diagenesis of the Tensleep Sandstone occurred shortly after deposition. For the most part, this is evidenced by anhydrite-gypsum and dolomite cementation (Figure 2.10). This cementation was followed by silica and dolomite cementation which occured before oil migration. This cementation was probably related to changes in the basin hydrology during regional downwarping in the Jurassic. The Laramide orogeny not only caused major hydrocarbon entrapment, but also caused calcite pore fillings and anhydrite and silica fracture fillings. They also analyzed surface and subsurface water to detect calcite stability. Calcite is the stable phase at the surface and in the subsurface to the south where down-dip flow of surface waters occurs in the eolian upper Tensleep sand.

A study done by Akhtar (1991) in South Casper Creek oil field, Wyoming, supports the ideas of Mankiewicz and Steidmann (1979). Akhtar (1991) emphasized that diagenesis of Tensleep Sandstone was controlled by its depositional facies. Each lithofacies with its characteristic mineral composition and sedimentary structures was deposited in a different depositional environment. These lithological characteristics strongly influenced diagenetic alteration that subsequently occurred in the Tensleep Sandstone.

Figure 2.10

2.3 Structural Geology

2.3.1 Regional Structure

2.3.1.1 Lineaments

Lineaments are important structural elements in the Bighorn basin. Hoppin (1974) defined lineaments as generally rectilinear lines or zones of structural discordance of regional (60 mi, 100 km or more) extent. They are expressed at the surface by alignments of combinations of linear features which can be of several types. In other words, lineaments are manifested at the surface in many diverse ways. For example, single large faults, groups of fault which are subparallel to the lineament trend, en-echelon oblique fault and fold belts, large monoclines, and juxtaposition of blocks of contrasting structure and lithology can all occur.

Faults and anticlinal folds are shown in Figure 2.11 (Hoppin and Jennings, 1971). Figure 2.12 shows the lineaments proposed by Hoppin (1974). Six major lineaments are developed in the Bighorn basin.

The Nye-Bowler lineament, first described by Wilson (1936), is located at the far north end of the Bighorn basin. Its length is about 109 mi (175 km) and the feature

Figure 2.11

Figure 2.12

extends from Livingston, Montana, to the east front of the Pryor Mountains. It is an alignment of folds, laccoliths, and parallel and en-echelon faults.

The Tongue River lineament was originally described by Demorest (1941). This zone includes fault zones of intense fracturing with retrograde metamorphism, silicification and mineralization and geographic linears.

The Shell lineament was proposed by Hoppin and Jennings (1971). Mineralization and fault zones occur along this trend. Extension further west is questionable, but hot springs in the Cedar Mountain area are located at the continuation of this trend.

The Florence Pass lineament was first recognized by Hodgson (1965). The Alkali fault, the subject of this study, is one part of this lineament. He described it as an en echelon series of relatively straight valleys in the Precambrian core. He also showed that 490 ft (150 m) of down to the north faulting occurs west of Florence Lake. On the west flank, the lineament is represented by locally faulted monoclinal flexures. The Florence Pass lineament cuts Precambrian-aged rocks in the Bighorn Mountains. It appears in Paleozoic rocks in the study area.

The well known Tensleep lineament is located south of the Florence Pass lineament. Wilson (1938), Hoppin et al. (1965), and Hodgson (1965) mapped the east-west trending Tensleep fault, and saw that the Tensleep fault, which is a dip-slip fault, turns into a monoclinal structure to the west.

The Thermopolis lineament was proposed by Hoppin and Jennings (1971). It includes an east-west zone of faults and folds in the southern Bighorn basin, passing through the hot springs at Thermopolis.

2.3.1.2 Laramide Orogeny

The Laramide Orogeny is a series of mountain-building events that affected much of western North America during the Late Cretaceous and Early Tertiary. Events ascribed to the Laramide range in age from Late Cretaceous to as late as Oligocene (68 Ma-23 Ma) (Bird, 1984, 1988; Chapin and Cather, 1981; Hamilton 1981). Evidence of the Laramide Orogeny is present from Mexico to Alaska, but the main effects appear to be centered in the eastern portion of Cordilleran geosyncline from southern Nevada to the Northern Rockies (Hamilton, 1988). This includes the central Rockies of Montana and Wyoming, the southern Rockies of Colorado and New Mexico, and southern Arizona.

In pre-Laramide Cretaceous time, when convergence was relatively slow, an accretionary wedge of melange, a fore-arc basin, a magmatic arc and foreland thrust belt was produced (Hamilton, 1978). Toward the end of Cretaceous time, convergence accelerated, the lithosphere being subducted was younger and sank more slowly, arc magmatism spread far inland, and Laramide deformation began. Near the end of the Eocene epoch (about 40 Ma), the Rockies again were uplifted several thousands of feet and volcanoes erupted, most extensively in the Yellowstone plateau and Absaroka Range.

The last uplift occurred just before the Pleistocene epoch about 2 million years ago (Hamilton, 1981). From that time, topography was shaped by rivers that cut canyons and deep gorges through the ranges. Another factor was glaciers that formed during the Ice Age and moved down the valleys and further eroded the mountains.

The Laramide Orogeny (Figure 2.13) consists of great eastward-directed thrust faults and folds with only slight basement involvement in the western portion of the Cordilleran Geosyncline (Hamilton, 1988). In addition, coarse clastic basin sediments and unconformities formed in the central and southern Rockies, along with acidic plutonic intrusions ranging in age from 50 Ma to 70 Ma.

The Laramide compressive deformation of the craton was caused by a clockwise rotation of about 2 to 4 degrees of the Colorado Plateau region, during the late Cretaceous and early Tertiary time (Hamilton, 1981). During that time, the time of Laramide orogeny, the approximate direction of relative convergence between North American and Faralon plates was southwest-northeast. This convergence caused N57E stress direction in Bighorn basin (Hamilton, 1981).

The Laramide Orogeny is a typical example of a low-angle convergent plate boundary (USGS website). Figure 2.14 demonstrates that the angle of the subducting plate is significantly flatter (around 10 degrees), moving the focus of melting and mountain building much farther inland than is normally expected.

Bird (1998) described the kinematic history of the Laramide Orogeny between latitudes 35- 49 N (Figure 2.15). The Laramide Orogeny occurred from 75-35 Ma, with

Figure 2.13

Figure 2.14

Figure 2. 15

peak Colorado Plateau velocities of 1.5 mm/yr during 60 – 55 Ma. The main azimuth of foreland velocity and mean direction of foreland shortening was stable at 40 degrees for most of the orogeny, increasing to 55 degrees from 50-40 Ma. He also demonstrated that the Laramide Orogeny had a different mechanism than the Sevier Orogeny. The Laramide Orogeny was driven by basal traction during an interval of horizontal subduction, not by edge forces due to coastal subduction or spreading of the western cordillera or by accretion of terranes to the coast.

2.3.1.3 Intermontane Basins of Wyoming

Information about intermontane basins of Wyoming has been summarized from the following websites: 1- Geography of Wyoming, 2- NASA.

The late stages of development of the western Cordillera (Laramide Orogeny) produced intermontane structural basins and adjacent mountain blocks in the foreland. This style of foreland deformation is the typical signature of continental plates adjacent to a convergent margin of long duration, instead of continent/continent collisions. This type of collision produced a pattern of compressive uplifts and basins, with most of the deformation confined to the block edges. The basin contains several thousand meters of Paleozoic and Mesozoic sedimentary rock that predate the Laramide Orogeny. As much as 16,400 ft (5,000 m) of Cretaceous and Tertiary sediments filled these basins. Also deformation in Paleocene and Eocene deposits record continuing orogenic activity.

Intermontane basins occur principally in the central Rocky Mountains from Colorado and Utah (Uinta basin) to Montana and are best developed in Wyoming, with the Bighorn, Powder River, and Wind River basins being the largest. Paleozoic and Tertiary units in these basins dip from the margins into the basin centers. Also, these basins are surrounded by mostly Precambrian-aged rocks, and thrust or reverse faults. Some boundaries seem to be monoclinal features, and faulting is covered by recent sediments.

Most faults show evidence of both thrust and strike-slip types of displacement in the intermontane basins of Wyoming. These suggest that at least two episodes of Laramide movement occurred during the Late Cretaceous and Eocene.

Drainage of the Wyoming basins is problematical because rivers seem to disregard the structures. The Sweetwater River cuts across the Wind River Range and Sweetwater Mountains. The Bighorn River takes a difficult course across the Owl Creek Mountains. The Green River has eroded a deep canyon through the Uinta Mountains.

2.3.1.4 Bighorn Basin

The Bighorn basin, which is a large intermontane basin, approximately covers 10,000 mi^2 (25,900 km^2) (Figures 2.16, 2.17). The Bighorn Mountains are about 120 mi (192 km) long and 25 to 30 mi (40 to 48 km) wide.

Figure 2.16

Figure 2.17

Many areal mapping and structural studies have been focused along the flanks of the range where both the Precambrian basement and overlying Paleozoic and Mesozoic sedimentary rocks were deformed during Laramide tectonism.

The Bighorn basin is surrounded by the Beartooth Mountains to the northwest, the Pryor Mountains to the north, the Bighorn Mountains to the east and the Owl Creek Mountains to the south. The Montana Lineament, whose direction is transverse to the basin, is located at the northern boundary of the basin between the Pryor and Beartooth Mountains. The Absaroka volcanics cover the western margin of the basin.

The general structure of the Bighorn basin was originally described as a large, fairly simple, major syncline with marginal folds by Fisher (1963). Detailed mapping, drilling, and extensive seismic work reveal far more complex structural patterns. A proposed structural interpretation of the deformation of the Bighorn basin and its vicinity is presented by Curry (1983). Deformation occurred as a result of eastward and westward moving of mantle convection currents, which met in the cordillera and sank into the deeper mantle. Part of the proposed mantle convection current system flowed southwestward across Wyoming and tilted large segments of the brittle crust into downwarped basins, such as the Bighorn basin. When the large crustal plates were tilted during the Laramide Orogeny (middle Paleocene through Eocene), smaller crustal blocks were tilted and rotated.

Figure 2.18 shows three types of regional gravity features, which are: gravity lows in the basins, gravity highs in the mountain uplifts, and a zone of steep gravity

Figure 2.18

hingeline between the uplifts and basins (Curry, 1983). A profile of the regional gravity field across the Bighorn basin is shown along cross section A-B in Figure 2.19.

Curry (1983) compared the gravity lows (Figure 2.20) to the axes of the Bighorn, Powder River and Wind River basins. These gravity lows overlie the basin axes. The extension of the gravity lows to the northwest of the mapped basins suggest northwest extensions of the basins. Curry (1983) also demonstrated that gravity highs around the Bighorn basin coincide with outcrops of Pennsylvanian and older rocks, such as those in the Bighorn and Beartooth Mountains.

2.3.2 Local Structure

There are two main local structures in the general general study area, which are the Tensleep fault and the Alkali fault.

2.3.2.1 Tensleep Fault

The Tensleep fault is an east-west trending dip-slip fault (Darton, 1904; Wilson, 1938; Hoppin et al., 1965; Hodgson 1965). The fault is covered by Tertiary deposits in

Figure 2.19

Figure 2.20

the Bighorn basin. Hodgson (1965) stated that the structure extends entirely across the basin. There is no surface evidence of its presence under Tertiary deposits of the Powder River basin to the east. He stated that the north side of the fault moved up from 500 to 1000 ft (152 to 305 m) as result of the monoclinal character of the structure.

The Tensleep fault was originally treated as a normal fault, down to the south by Wilson (1938). Wilson (1938) concluded that the fault occurred along pre-existing lines of weakness in the basement complex. This was re-activated by Laramide deformation. Hoppin's (1965) study showed that the fault is controlled by anisotropy in the Precambrian basement. Blackstone (1986) stated that the Tensleep fault is a reverse fault with the north side up. It may have been modified by later normal faulting. Allison (1983) made the opposite interpretation. He also claimed that the fault moved in two phases, the latter phase having reverse fault character. All of these works show that the Tensleep fault has had more than one phase of movement, but the sense of offset is still unclear. The sketch in Figure 2.21 shows the last known movement on the fault. The throw on the Tensleep fault is drawn based on Wilson (1938) and Allison (1983).

Hoppin and Jennings (1971) detected fold position in the area. They defined fold asymmetries on either side of the Tensleep fault differently. Steep northeast limbs of anticlines occur to the north of the Tensleep fault and steep southwest limbs of folds occur to the south.

Figure 2.21

2.3.2.2 Alkali Fault

The Alkali fault is part of the Florence Pass lineament, which was first recognized by Hodgson (1965) by means of a reconnaissance geologic study. He described the west part of the Florence Pass lineament as a big monocline, which is locally faulted and has an average structural relief of 200 ft (61 m). The eastern part of this structure is expressed topographically as an en echelon series of relatively straight valleys. Hoppin and Jennings (1971) worked on folds north and south of the Florence Pass lineament. They found that folds to the south of the lineament are asymmetric (steep limb) to the northeast. Folds to the north of this lineament are asymmetric to the southwest.

The Alkali fault is a major east-west trending (Figure 2.22) fault that cuts the Tensleep Sandstone. The north side of the fault has moved up approximately 40 ft (12 m). Dip-slip displacement was measured by tracking the contact at the base of the Tensleep Sandstone. Chapter 3 discusses the inferred principle stress direction of the area based upon observed shear fracture sets. Position of the maximum principle stress supports the fact that the Alkali fault may have been a left-lateral strike slip fault with some dip-slip offset.

Figure 2.22

The Alkali fault is very distinctive in the study area. Sedimentary rocks are brecciated and crushed for a distance of about 3 ft (1 m), and locally more along the fault. The Alkali fault can be followed to Medicine Creek to the east of the study area**.** There is no surface expression on the other side of the canyon, which is covered by Tertiary deposits. In the west, it was enclosed by vegetation, and cannot be traced on the surface.

2.4 Petroleum Geology

The Bighorn basin, which is one of the most prolific Rocky Mountain basins, has eight oil fields which are greater than 100 million bbl of oil in size. Some production statistics appear in Table 2.1. The basin includes carbonate and siliciclastic strata as thick as 25,000 ft (7,620 m). Most of the oil fields result from faulting and folding at the basin margin.

Production in the Bighorn basin is mostly from the Pennsylvanian Tensleep Sandstone, Permian Phosphoria Formation, Cretaceous sandstone reservoirs, and Ordovician, Devonian and Mississippian-age carbonate reservoirs. Exploration plays are aimed at the sub-Absaroka, based on structural traps in Paleozoic reservoirs beneath the Lower Tertiary Absaroka Volcanic supergroup on the west flank of the basin. Deep basin structural and stratigraphic plays, primarily for gas, are based on the occurrence of deep anticlinal structures in the basin center and isolated sandstone reservoirs of Cretaceous

Table 2.1 Production from 8 giant oil fields of the Bighorn basin. Adapted from Peterson (1990).

OUTPUT OF BIGHORN BASIN FIELDS

Field	Discovery Date	Size (MMBO)	Cumulative Production Jan. 1, 1988 (MMBO)
Elk Basin	1915	530	500
Oregon Basin	1912	410	380
Hamilton Dome	1918	270	265
Grass Creek	1914	195	183
Garland	1906	160	153
Byron	1918	130	120
Little Buffalo Basin	1914	127	115
Frannie	1928	120	115

and Tertiary age. Also, Permian-age isolated carbonate buildups have potential for deep gas reservoirs.

The Permian Phosphoria Formation, which contains organic-rich phosphatic shales, is the source rock for these oil deposits. Sheldon (1967) and Claypool et al. (1978) claimed that Phosphoria oil formed in western Wyoming and migrated as far as the eastern Powder River basin. Maximum burial of Permian strata though most of the basin occurred at the end of the Cretaceous period.

The estimates of undiscovered conventional resources for the Bighorn basin range from about 100-490 million bbl of oil and 180-1590 bcf (billion cubic feet) of gas (USGS).

Chapter 3

SCANLINES

3.1 Introduction

Exposures of the Tensleep Sandstone at Alkali Creek provide an excellent opportunity to investigate fracture networks in an eolian depositional system.

In this chapter, data collection methods are first explained. Second, fracture sets in the study area are determined by analyzing the fracture data with reference to fracture sets which have studied by other workers. In this way, local fracture sets and regional fracture sets could be differentiated from each other. Finally, fracture lengths were determined for each fracture set.

3.2 Data Collection Methods

Field studies were conducted at Alkali Creek during the summer of 2000. During this period, data were collected using following methods.

A Trimble Pathfinder PRO / XRS GPS receiver system was used to detect the location of scanline surveys and the Alkali fault (Figure 3.1). The Trimble Pathfinder PRO / XRS consists of a GPS receiver system, antenna, and data logger, which is a hand-held computer used to store field data. The data logger works with a receiver system and antenna (Figure 3.2). Pathfinder Office software provides uploading and downloading capabilities.

Fracture orientations were determined using orthogonal scanline measurements, and pavement mapping at various locations. Scanline pairs 1-2, 5-6, 7-8, 13-14 were not orthogonal because of outcrop restrictions. Scanline surveys were located at 20 different spots at different distances from the fault. In addition to this, 234 fracture strikes and dips were taken between scanlines 15 and 18 (Figure 3.1) at a very close distance, 12 m (40 ft) or less from the Alkali fault. Fracture strike and dip data were plotted on lower hemisphere equal area Schmidt nets for statistical analyses.

All orientation data are given using the right hand rule convention. To use the right-hand rule when measuring strike with a compass, always keep the dip direction to the observer's right, as though he was looking at his right hand, palm side up, and his right thumb was pointing to the "down-dip" side. Using this method of recording data will consistently record the dip direction in a clockwise rotation relative to strike. Conventional dip and dip direction measurements appear in Appendix A. Scanline locations are shown in Appendix B.

Figure 3.1

Figure 3.2

A scanline survey is a basic method used to acquire fracture data in a systematic way (Baecher, 1983). To do a scanline survey (Figure 3.3), a measuring tape, not less than 25 ft (8 m) in length, is laid on the outcrop. The fractures longer than some threshold, such as 6 ft (2 m), are recorded. Strike and dip, length of the fracture, offset, filling type, distance from end of the scan-line, and facies are recorded for each fracture (Appendix A). Also, scanline orientation, length and scanline distance to the fault are recorded to better understand the fracture orientation. Fracture terminations are described as bed, outcrop, rock, or T junction (Figure 3.3). In addition to this, approximately 30 strikes and dips of fractures were measured not more than 75 ft (25 m) away from each pair of scanline surveys to improve the statistical analysis.

To better describe the fracture network, pavement maps were constructed at different spots along the Alkali fault. A pavement map is a visualization tool of fracture networks which helps determine fracture spacing, density, length, and truncation relationships.

Figure 3.3

3.3 Fracture Description

3.3.1 Modes of Fracture Formation

Fractures occur in association with faults, folds and other shear zones. Although three kinds of fractures have been described, they can be summed up under the title of the joints and shear fractures.

Joints, also known as Mode 1 fractures, are extensional fractures that had no appreciable movement parallel to the fracture direction, and only slight movement normal to the fracture plane (Figure 3.4a). In other words, offset occurs only parallel to the fracture plane by opening the fracture.

The other types of fractures are shear fractures. Shear fractures can be both Mode 2 fractures (Figure 3.4b) that occur by a tearing motion along the fracture, or Mode 3 fractures (Figure 3.4c) that formed by sliding motion along the fracture.

3.3.2 Fracture Sets

Fracture orientations were determined from scanline measurements and pavement mapping. Fracture strike and dip data for each pair of scanlines with 30 random measurements were plotted on lower hemisphere equal area nets for statistical analysis. All orientation data are given in the right-hand rule convention (facing the strike azimuth, dip is to the right). Dip measurements can be found in Appendix A.

Figure 3.4

Fracture strike and dip data are plotted and contoured by using the default algorithm of “StereoNet 3.0” which belongs to the Geological Software company.

Six fracture sets occur in the study area. These sets are defined by plotting strikes and dips from scanlines and random measurements on lower hemisphere equal area nets. The main reason for plotting 30 random measurements with the scanline measurements is that the number of fractures coming from the scanlines is limited. Because of this, the stereonets are considered useful for fracture set determination. The scanlines are more useful for fracture spacing information.

Sets 1, 4, 5, and 6 are detected from each stereonet plotted for each pair of scanlines including 30 random measurements. Sets 2 and 3 are detected from Figure 3.14, which shows random strike and dip measurements within 40 ft (12 m) of the Alkali fault. Except for scanlines 9, 10, 11, and 12, fracture set 1 is detected for every scanline.

Because of the different N values, the contour diagrams came out with different percentage rates. For this reason, different cutoff percentages are used for each density grid.

Sets 1 and 5 are detected with a 4.8% cutoff from the density grid of scanlines 1 and 2 (Figure 3.5). Sets 1, 3, 4, and 6 are detected with a 4.1% cutoff from the density grid of scanlines 3 and 4 (Figure 3.6). Sets 1, 4, 5, and 6 are detected with a 4.3% cutoff from the density grid of scanlines 5 and 6 (Figure 3.7). Sets 1 and 2 are detected with an 8.2% cutoff from the density grid of scanlines 7 and 8 (Figure 3.8). Sets 4 and 5 are detected with a 4.2 % cutoff from the density grid of scanlines 9 and 10 (Figure 3.9). Sets

Figure 3.5

Figure 3.6

Figure 3.7

Figure 3.8

Figure 3.9

2 and 6 are detected with a 6.8% cutoff from the density grid of scanlines 11 and 12 (Figure 3.10). Sets 1 and 4 are detected with an 8.5% cutoff from the density grid of scanlines 13 and 14 (Figure 3.11). Sets 1, 5, and 6 are detected with a 5.1% cutoff from the density grid of scanlines 15 and 16 (Figure 3.12). Sets 5 and 6 are detected with a 7.7% cutoff from the density grid of scanlines 17 and 18 (Figure 3.13). Sets 1, 3, 4, and 5 are detected with a 6.7% cutoff from the density grid of scanlines 19 and 20 (Figure 3.14).

On the upper part of Figure 3.15, all scanlines and the random measurements are plotted on a Schmidt equal area lower hemisphere projection. Fracture sets 1, 4, 5, and 6 are apparent with a cutoff of 2.5%. Sets 2 and 3 are much more clear on the lower Schmidt equal area lower hemisphere projection, which shows strikes and dips within 40 ft (12m) of the fault. In this density grid, Sets 1, 2, and 3 are detected with a 5.1% cutoff.

Fracture Set 1, which is an extensional fracture set, is the dominant set in the region with an average orientation of 226/80. Set 2 and 3 fractures are interpreted as conjugate shear fractures with an average orientation of 251/ 84 and 205/87, respectively.

Sets 4 and 5 fractures are orthogonal to each other and have approximately 90 degree dip angles. The average orientation of Set 4 is 273/88 and Set 5 is 182/87. Set 4 is developed as a deformation band near the fault with very close spacing.

Set 6 has an average orientation of 124/78. This fracture set is orthogonal to Set 1, which can be traced all over the Bighorn basin.

Figure 3.10

Figure 3.11

Figure 3.12

Figure 3.13

Figure 3.14

Figure 3.15

3.3.3 Fracture Fillings

At Alkali Creek, most fractures, especially those close to the fault, are healed by calcite. Sets 5 and 6 are the unfilled fracture sets of the study area. Fracture sets 1 and 4 are partially healed in the study area. Close to the fault, most fractures are oriented northeast-southwest. Although fracture sets 2 and 3 are all healed, set 1 fractures can be found both open and healed by calcite. Fracture set 4 consists of deformation bands near the fault. Some set 4 fractures are open at a distance greater than 200 ft (61 m) from the Alkali fault.

A deformation band (Figure 3.16a) is a thin zone of crushed grains caused by a small offset which can be on a scale of 1 mm to 1 cm (Antonellini and Aydin, 1995). A zone (Figure 3.16b) is comprised of many deformation bands localized near each other accommodating a total cumulative offset of a few decimeters. A slip plane (Figure 3.16c) is a surface of discontinuity accommodating offset of a few meters or larger. Slip surfaces are always associated with zones of deformation bands (Antonellini and Aydin, 1995).

Figure 3.17, taken from the Alkali fault zone, shows a zone of deformation bands. Based on Antonellini and Aydin (1994), permeability decreases by a factor of one to four times normal to the deformation bands, depending on the host rock porosity.

Figure 3.16

Figure 3.17

Figure 3. 18 shows a thin section of a deformation band from Tensleep outcrops at Ziesman Dome, Wyoming (Aviantara, 2000). The deformation bands, which are approximately 0.2 mm wide, exhibit grain size and volume reduction from cataclasis.

3.4 Fracture Length

It is difficult to define fracture length in the study area because of recent alluvium, which covers the fractures. Therefore, most of the outcrop fractures terminate due to incomplete exposure. In other words, most fracture lengths are minimum fracture lengths.

Fracture lengths are investigated by building histograms. The lengths for sets 1, 5, and 6 are generally between 0-10 ft (0-3 m) (Figures 3.19, 3.23, 3.24). The longest fracture length for these sets is 40 ft (12 m). The lengths for sets 2 and 3 are between 10-20 ft (3-6 m) (Figures 3.20, 3.21). Fracture length for fracture set 4 is between 0-10 ft (0-3 m) (Figure 3.22). Although the average fracture length for set 4 is less than 10 ft (3 m), individual fractures are locally longer than 50 ft (15 m), especially near the fault. This set mainly contributes to the deformation band type of fractures.

Fracture lengths for observed fracture sets are generally between 0-20 ft. For modeling purposes in the next chapter, arbitrary 100 ft (30 ft) fracture lengths are used. This is an attempt to account for the fact that most fractures are terminated because of incomplete outcrop exposures.

Figure 3.18

Figure 3.19

Figure 3.20

Figure 3.21

Figure 3.22

Figure 3.23

Figure 3.24

3.5 Discussion

Figure 3.25 shows wrench-fault related structures. There are two factors that control the structures: (1) the evolutionary stage or magnitude of the wrench faulting; (2) the structural response of the deformed terrane (Harding, 1974). This figure shows the relationship of expected fault and fold orientations with regard to maximum principle stress. Harding's (1974) model supports the idea that the Alkali fault might have a left-lateral strike-slip component (Figure 3.26). There is no obvious surface evidence observed for a left-lateral strike slip fault at the Alkali fault. Assuming that set 1 fractures are extension fractures that are parallel to maximum principle stress, the stress angle is apparently 46˚ from the north. Therefore, most of the stress transmits to the fault plane laterally. The second important concept in Harding's (1974) model is that anticlines and reverse faults occur perpendicular to the maximum principle stress. Normal faults and extensional fractures lie parallel to the maximum principle stress direction (Figure 3.25).

The stress direction is 57˚ in the Bighorn basin, according to Hamilton (1981). Although the stress direction differs by 11˚, the result coming from this study generally agrees with the Hamilton (1981) study.

Sets 1, 2 and 3 fractures can be seen in a diagrammatic sketch in Figure 3.24. In this model, the extension fractures (set 1) lie parallel to the direction of maximum compressive stress and perpendicular to the minimum compressive stress. Conjugate shear fractures (sets 2 and 3) formed at an acute angle to the maximum compressive

Figure 3.25

Figure 3.26

stress direction. The angle between shear fractures, called the conjugate angle, is 46˚. The conjugate angle in most cases is around 60˚. This can vary, primarily depending on mechanical properties of the sandstone and the magnitude of minimum compressive stress.

The other important concept is fracture fillings. Fracture set 1 occurs as extensional fractures that are healed in the vicinity of the Alkali fault. This is because sets 1, 2, 3 fractures and deformation bands, which is part of fracture set 4, occurred with fault movement. After these fractures were generated, diagenesis might have occurred in the area. This is why fracture set 1 is healed, although it is an extensional fracture. During the Bighorn basin development, fracture sets 4, 5, 6 and part of set 1 occurred as regional fractures which are seen as open fractures in the entire Bighorn basin.

Fracture sets in the Bighorn basin have been studied by various scientists. The main question concerns the effect of the Precambrian basement structure on the overlying strata. In other words, how do faults and fractures in Paleozoic rocks relate to Precambrian structures?

Hodgson (1965) published a reconnaissance fracture study in the Bighorn Mountains. Figure 3.27 shows the fracture sets in Precambrian rocks of the northern

Figure 3.27

Bighorn Mountains. Most of the fracture sets in the Tensleep Sandstone have a similar orientation to fractures in Precambrian basement (Figure 3.28).

Figure 3.28

Chapter 4

COMPARTMENTS

4.1. Introduction

Fractured reservoirs account for 21 billion barrels of oil equivalent in oil and gas fields operated by British Petroleum (Nelson, 2001). However, people in industry commonly deny the presence of fractures in reservoirs.

Ignoring fractures can cost time and money. It causes irreparable loss of recovery, primary recovery patterns that are inappropriate for second recovery, and improper assessment of economics.

The solution is to determine the effect of natural fractures in our reservoirs as early as possible to evaluate each reservoir correctly from day one. In many cases, finding the fractures is not enough. Fractured reservoirs are very complicated and difficult to evaluate.

For this reason, in this chapter, compartmentalization that occurs as a result of healed fractures and second-order bounding surfaces in eolian sandstone is discussed and its effect on reservoir productivity is emphasized.

4.2. Fracture Spacing

Fracture spacing is an important parameter needed to predict fracture porosity and permeability in a reservoir. Variation in fracture spacing can have a dramatic effect on both fracture porosity and permeability. In this text, fracture spacing is defined as the average distance between regularly spaced fractures measured perpendicular to a parallel set of fractures of a given orientation. This method was first used by Parson (1966).

In scanline surveys, three geometric properties are commonly of interest: fracture spacing, fracture length, and fracture orientation. Fracture spacings are investigated for each set by building histograms and computing mean spacing at different distances from the Alkali fault. Fracture sets 1, 2, and 3 are the main fracture sets in which the intensity decreases when going away from the fault. Fracture sets 2 and 3 are interpreted as conjugate shear fractures near the fault. At a distance from the fault, this conjugate effect is reduced and sets 2 and 3 are rarely seen. Fracture spacings in sets 2 and 3 are less than 1 ft (0.3 m) within 40 ft (12 m) of the fault. These fractures are healed by calcite. Spacing increases to 7 ft (2.1m) for set 2 and 8 ft (2.4 m) for set 3 at a 400 ft (122 m) distance from the fault (Figures 4.3 and 4.5).

The most dense fractures within 40 ft (12 m) of the fault comprise fracture set 1. Fracture spacing for set 1 dramatically increases with distance from the fault (Figure 4.1). Spacing is around 1 ft (0.3 m) near the fault, but it changes to 19 ft (5.8 m) at a 1,500 ft (457 m) distance from the fault.

Fracture set 4 is seen as deformation bands (gouge-filled fractures) near the fault. When going away from the fault, fracture spacing changes from 1 ft (0.3 m) to more than 10 ft (3 m) (Figure 4.7). Fracture filling becomes open.

Fracture sets 5 and 6 apparently are not related to the Alkali fault (Figures 4.9 and 4.11). Although different fracture spacings are measured at each scanline location, mean fracture spacing for these fracture sets is 9 ft (2.7 m).

Fracture spacing histograms are shown in Figures 4.1, 4.3, 4.5, 4.7, 4.9, 4.11 at the bottom. Appendix B shows the spreadsheet from which these plots were generated. These histograms show that fracture sets 1, 2, 3, and 4 have fracture spacing less than 2 ft in the vicinity of the fault. Except for this, other fracture spacings are dispersed. Fracture spacing for sets 5 and 6 generally range from 7-9 ft (2.1-2.5 m).

Areal fracture patterns with a constant 100 ft (30 m) fracture length are shown in Figures 4.2, 4.4, 4.6, 4.8, 4.10, and 4.12. A parallelogram shape was chosen that was elongated roughly in the set 1 fracture direction.

Figure 4.1

Figure 4.2

Figure 4.3

Figure 4.4

Figure 4.5

Figure 4.6

Figure 4.7

Figure 4.8

Figure 4.9

Figure 4.10

Figure 4.11

Figure 4.12

4.3. Flow Compartment Areas

One of the main purposes of this thesis is to measure fracture compartment area as a function of distance from the Alkali fault. To delineate the compartments, I built a 2D fracture model of the study area.

Four of six fracture sets are healed in the study area. Fracture sets 2 and 3, the shear fractures, are healed. Fracture set 1 is mostly healed close to the fault, but open fractures are common. Therefore, in the fracture model, there are more closed fractures close to the fault than away from the fault. Fracture set 4 has deformation bands near the fault, but the fractures beyond 200 ft (61 m) from the fault are open fractures. Therefore, set 4 fractures within 200 ft (61 m) of the fault are considered to be healed fractures.

Mean fracture lengths for the fracture sets are restricted between 0-20 ft (0-6 m) (Chapter 3). Therefore, an arbitrary 100 ft (30 m) fracture length is used in the models. Most of the time, fractures in the study area are terminated by vegetation or soil, which do not allow me to measure the fracture length properly. Therefore, fracture lengths, coming from these fractures, are minimum lengths. In addition, because of the diverse orientations of fracture sets, compartmentalization is controlled more by spacing than by length. Fracture spacing is typically on the order of 10 ft (3 m) or less for fracture sets 1, 2, and 3. Therefore, an arbitrary fracture length of 100 ft (30 m) is at least one order of magnitude greater than the mean fracture spacing. I believe this will give valid fracture compartment areas.

4.4. Second-Order Bounding Surfaces

Brookfield (1977) identified three orders (first, second and third order) of bounding surfaces in eolian sandstones based on their extent and regularity. These form at different scales as a direct consequence of migrating trains of bedforms of different hierarchy.

First-order bounding surfaces are subhorizontal, regionally extensive, low relief planes that cut across all underlying eolian cross stratification and lower rank bounding surfaces (second- and third-order bounding surfaces). In the study area, first-order bounding surfaces separate large-scale tabular-planar eolian cross-stratified sets (Aviantara, 2000).

Second-order bounding surfaces are also called second-order surfaces, superposition surfaces (Kocurek, 1996), or stacking surfaces (Fryberger, 1990). They lie between the first-order surfaces and separate bundles of eolian cross-strata sets. The process that forms these surfaces is the passage of dunes across draas (Brookfield, 1977 and 1992) or the migration of superimposed smaller scale dunes across the lee face of main bedforms (Kocurek, 1996).

Third-order surfaces are the reactivation surfaces that bound eolian cross strata sets. They are formed by minor fluctuations in the wind direction or speed which results in ceased deposition or minor local erosion for a short period of time.

Carr-Crabaugh and Dunn (1996) sampled bounding surfaces in outcrop and subsurface to measure directional oil-water relative permeability. The result is fluid flow being significantly lower across the bounding surfaces than parallel. Baffling occurred across the second-order bounding surfaces, in which permeability decreased between 14 to 40 times across the surfaces.

Figure 4.13 shows the second-order bounding surfaces of the study area. These were created as flat surfaces, although, they are known to be curved both in dip and strike direction (Ciftci, 2001).

4.5. Compartmentalization

Although the Tensleep Sandstone has original oil in place volumes in the billions of barrels, recoveries are commonly not more than 15% in some fields (Peterson, 1990). These low recovery factors are the direct result of reservoir heterogeneity caused by permeability anisotropy, depositional compartmentalization, fractures, and diagenesis. Besides regional fractures, reservoirs in the Tensleep Sandstone have local fractures caused by faults and folds.

Figure 4.14 shows the fracture patterns of the study area. To show the compartmentalization caused by fractures and second-order bounding surfaces as a function of distance from the Alkali fault, only healed fractures are used. Three sample boxes are defined in Figure 4.15, which shows healed fractures of the study area. By

Figure 4.13

Figure 4.14

Figure 4.15

calculating the area of the compartments in each square, the area of the compartmentalization at a distance from the Alkali fault is detected. Area calculation was done by hand after taking enlarged scaled printouts of these boxes. In compartment area calculations, only complete compartments were used. Compartments truncated by the edge of the box were ignored. I counted 30 compartments in each box. The shape of compartments is divided into triangles for easy calculation.

After computing the midpoint of each square, the compartment's area is plotted. As seen in Figure 4.16, area of the compartments close to the Alkali fault is very small, between 1-20 ft^2 (0.1-1.9 m^2). They get larger and larger with distance from the fault. The compartment areas are around 249 ft^2 (23 m^2) at 500 ft (152 m) and 5,560 ft^2 (517 m^2) at 1,000 ft (305 m) distance from the fault.

Table 4.1. Summary of compartment areas.

	Compartments	Mean (ft^2)	Medium (ft^2)
Box 1	30	7	6
Box 2	30	249	225
Box 3	30	5560	5285

Figure 4.16

4.6. Discussion

One purpose of this thesis was to see the effects of the fracture system on fluid flow. Another goal was to combine fracture data with bounding surfaces to discuss the effect of drilling a well near a fault in an eolian sandstone.

At Alkali Creek, the fault is surrounded by mostly calcite filled fractures, which affect the reservoir permeability. Also, gouge-filled fractures are concentrated close to the fault.

Fractures with calcite filling (set 1) are dependent on diagenesis in the area. Deformation bands (gouge-filled fractures) developed as a result of movement of the fault. These deformation bands are closely spaced near the fault with approximately 1 ft (0.3 m) fracture spacing, and the intensity declines when going away from the fault.

Deformation bands reduce the porosity, grain size, sorting, and permeability of the fractured zone. In some cases, secondary mineralization further reduces the porosity and permeability. In addition, fine-grained deformed material possesses high water saturation that can drastically reduce the relative permeability to hydrocarbons.

One of the main results is that the Alkali fault caused compartmentalization in the study area by producing shear fractures and deformation bands. Compartmentalization is controlled by distance from the Alkali fault as a result of fracture intensity.

Figure 4.16 suggests that drilling a vertical well near the fault is not a good idea. Wells should be drilled at least 1,000 ft (305 m) from such faults to penetrate

compartments that are greater than 10,000 ft^2 (929 m^2) in area. A possible solution is horizontal drilling near the fault, perpendicular to fault strike. This way, highly compartmentalized sections of the reservoir could be connected to the well.

Chapter 5

CONCLUSIONS AND RECOMMENDATIONS

- GPS provides an accurate way to position faults and scanline locations on a map. By using GPS, the Alkali fault orientation is approximately N85E.
- Six main fracture sets are detected in the study area after plotting fracture strikes and dips on contoured stereonets. The average orientation is 226/80 for set 1, 251/84 for set 2, 205/87 for set 3, 273/88 for set 4, 182/87 for set 5, and 124/78 for set 6.
- Sets 1, 2, 3, and 4 are apparently controlled by the Alkali fault. Spacing gets larger with distance from the fault. Spacing changes from 0.5-11 ft (0.15-3.3 m) for set 1, 0.5-8 ft (0.15-2.4 m) for set 2, 0.5-8 ft (0.15-2.4 m) for set 3, 2-9 ft (0.6-2.7 m) for set 4, 4-9 ft (1.2-2.7 m) for set 5, and 4-8 ft (1.2-2.4 m) for set 6.
- Fracture set 4 is developed as deformation bands near the fault.
- Fracture sets 5 and 6 appear to be regional fracture sets of the Bighorn basin. Although there is some spacing variation close to the fault, both sets are consistent at a distance from the fault. These are open fractures.

- Fracture orientation helps determine principle stresses of the area. Fracture set 1 is the same direction as the maximum principle stress. Fracture sets 2 and 3 occur as conjugate fracture sets. The sense of offset on the Alkali fault is apparently left-lateral strike slip, with some amount of vertical offset.
- Average area of the compartments within 40 ft (12 m) of the fault is 7 ft^2 (0.7 m^2). The average compartment areas increase to 249 ft^2 (23 m^2) at 500 ft (158 m) and 5,560 ft^2 (517 m^2) at 1,000 ft (305 m) distance from the fault.
- Drilling near a strike-slip or oblique-slip fault is not a good idea in a Tensleep reservoir. Fault movement caused shear fractures and deformation bands to form near the fault. These fractures and deformation bands created permeability barriers and small compartments in the reservoirs.

REFERENCES

Aydin, A., 1978, Small faults formed as deformation bands in sandstone: Pure and Applied Geophysics, v. 166, p. 642-671.

Agatston, R. S., 1954, Pennsylvanian and lower Permian of northern and eastern Wyoming: AAPG Bulletin, v. 38, p. 503-583.

Akhtar, M.K., 1991, Diagenesis, porosity and permeability distribution in the Pensylvanian Tensleep Sandstone, South Casper Creek field, Natrona County, Wyoming: Unpublished Master's Thesis, Colorado School of Mines, Golden Colorado, 142p.

Allison, M. L., 1983, Deformation styles along the Tensleep fault, Bighorn basin, Wyoming: Wyoming Geological Association Guidebook, Bighorn basin, p. 63-75.

Ancestral Rockies, http://www.colorado-mall.com/HTML/EDUCATIONAL/SCIENCES GEOLOGY/COLO_CREATION/ANCESTRAL_ROCKIES/Ancestral_Rockies.html

Andrews, S., and Higgins, L. S., 1984, Influence of depositional facies on hydrocarbon production in the Tensleep Sandstone, Bighorn Basin, Wyoming: A working hypothesis: Thirty-Fifth Annual Field Conference, Wyoming Geological Association Guidebook, p. 183-197.

Antonellini, M., and Aydin, A., 1994, Effect of faulting on fluid flow in porous sandstones: Petrophysical properties: AAPG Bulletin, v. 78, p. 642-671.

Antonellini, M., and Aydin, A., 1995, Effect of faulting on fluid flow in porous sandstone: Geometry and spatial distribution: AAPG Bulletin, v. 79, p. 355-377.

Aviantara, A. A., 2000, Facies architecture of the Tensleep Sandstone, Bighorn basin, Bighorn County, Wyoming: Unpublished Ph.D. Thesis, The University of Tulsa, 249 p.

Baecher, B. G., 1983, Statistical analysis of rock mass fracturing: Mathematical Geology, v. 15, p. 329-348.

Bird, P., 1984, Laramide crustal thickening event in the Rocky Mountain foreland and Great Plains: Tectonics, v. 3, p.741-758.

Bird, P., 1988, Formation of the Rocky Mountains, western United States – A continuum computer model: Science, v. 239, p. 1501-1507.

Bird, P., 1998, Kinematic history of the Laramide orogeny in latitides 35° -49° N, western United States: Tectonics, v. 17, p. 780-801.

Blackstone, D. L., Jr., 1986, Foreland compressional tectonics: Southern Bighorn basin and adjacent areas, Wyoming: Wyoming State Geological Survey Report of Investigations 34, 32 p.

Boyd, D. W., 1993, Paleozoic history of Wyoming: *in* Snoke, A. W., Steidtmann, J. R., and Roberts, S. M., eds., Geology of Wyoming: Wyoming State Geological Survey Memoir 5, p. 164-187

Brookfield, M. E., 1977, The origin of bounding surfaces in ancient eolian sandstones: Sedimentology, v.24, p.303-332.

Brookfield, M. E., 1992, Eolian systems: *in* Walker, G. R., and James, N. P., eds., Facies models response to sea level change: Geological Association of Canada, p. 143-156.

Burgess, J. D. C., 1961, *Chaetetes* in the type section of the Tensleep Formation, Tensleep Canyon, Washakie County, Wyoming: Journal of Paleontology, v. 35, p.1222-1223.

Ciftci, N. B., 2001, Outcrop-based 3D modeling of the Tensleep Sandstone at Alkali Creek, Bighorn Basin, Wyoming: Unpublished Master's Thesis, Colorado School of Mines, Golden, Co, 272p.

Carr-Crabaugh, M., and Dunn, T. L., 1996, Reservoir heterogeneity as a function of accumulation and preservation dynamics, Tensleep Sandstone, Bighorn and Wind River Basins, Wyoming: DOE Contract No. DE-AC22-93BC14897, p. 10-36.

Christopher, J. S., and Randal, W. R., 1985, Recognition of interstitial anhydrite dissolution: A case of secondary porosity, San Andres Limestone, New Mexico, and upper Minnelusa Formation, Wyoming: AAPG Bulletin, v.69, p. 1064-1076.

Claypool, G. E., Love, A. H., and Maughan, E. K., 1978, Organic geochemistry, incipient metamorphism, and oil generation in black shale members of

Phosphoria Formation, western interior United States: AAPG Bulletin, v.62, p. 98-120.

Curry, W. H., 1983, A proposed structural interpretation of the Bighorn basin, Wyoming-Montana: Thirty-Fourth Annual field conference, Wyoming Geological Association Guidebook, p. 43-52.

Darton, N.H., 1904, Comparision of the stratigraphy of the Black Hills, Bighorn Mountains and Rocky Mountain Front Range: GSA Bulletin, v.15, p. 379-448.

Demorest, M., 1941, Critical structural features of the Bighorn Mountains, Wyoming: AAPG Bulletin, v.52, p. 161-176.

Desmond, R. J., Steidtmann, J. R., and Cardinal, D. F., 1984, Stratigraphy and depositional environments of the middle member of the Minnelusa Formation, central Powder River basin, Wyoming: *in* The Permian and Pennsylvanian Geology of Wyoming, Wyoming Geological Association 35th Annual Field Conference Guidebook, p. 213-239.

Duebenderfer, E.M., and Houston, R.S.,1986, Kinematic history of the Cheyenne belt, Medicine Bow Mountains, Southeastern Wyoming: Geology, v. 14, p.171-174.

Dunn, T.L., 1996, Anisotropy and spatial variation of relative permeability, and lithologic chracter of Tensleep Sandstone reservoirs in the Bighorn and Wind River Basins, Wyoming: D.O.E. Final Technical Report, Institute for Energy Research, University of Wyoming, Laramie, 174p.

Emmett, W. R., Beaver, K. W., and McCaleb, J. A., 1971, Little Buffalo Basin Tensleep heterogeneity-its influence on drilling and secondary recovery: Journal of Petroleum Technology, v. 23, p. 161-168.

Fisher, J. H., 1963, Tensleep Sandstone of the eastern Bighorn Mountains, Wyoming: Wyoming Geological Association – Billings Geological Society Joint Field Conference Book, p. 30-44.

Fox, J. E., Lambert, P. W., Mast, R. F., Nuss, N. W., and Rein, R. D., 1975, Porosity variation in the Tensleep and its equivalent the Weber Sandstone, western Wyoming: A log and petrographic analysis: 1975 Symposium, Rocky Mountain Association of Geologists, p. 185-216.

Fox, J. E., and Dolton, G.L., 1989, Petroleum geology of the Wind River and Bighorn basins, Wyoming and Montana: U.S.G.S Open-File Report 87-450P, 41p.

Fox, J. E., and Dolton, G. L., 1996, Petroleum geology of the Bighorn basin, north-central Wyoming and south-central Montana: Wyoming Geological Association 47th Guidebook, p.19-39.

Formation of Rocky Mountains, http://element.ess.ucla.edu/publications/1998_Laramide/1998_Laramide.htm

Geography of Wyoming, http://www.netstate.com/states/geography/wy_geography.htm

George, G. R.,1984, Cyclic sedimentation and depositional environments of the upper Minnelusa Formation, central Campbell county, Wyoming: Wyoming Geological Association Guidebook, 35 Annual Field Conference, p. 75-95.

Giles, R. B., 1980, Putting second recovery units together: Rocky Mountain Mineral Law Foundation on Pooling & Utilization of Oil & Gas Leases.

Goggin, D, J., Chandler, M. A., Kocurek, G., and Lake, L. W., 1992, Permeability transects of eolian sands and their use in generating random permeability fields: SPE Formation Evaluation, v. 7, p. 7-16.

Hamilton, W. B., 1978, Mesozoic tectonics of the western United States: Pacific Section, Society of Economic Paleontologists and Mineralogists, Pacific Coast Paleogeography Symposium 2, p. 33-70.

Hamilton, W. B., 1981, Plate-tectonic mechanism of Laramide deformation: University of Wyoming Contributions to Geology, v. 19, p. 87-92.

Hamilton, W. B., 1988, Laramide crustal shortening: Geological Society of America, Memorial 171, p. 27-35.

Harding, T. P., 1974, Petroleum traps associated with wrench faults: AAPG Bulletin, v. 58, p. 1290-1304.

Harland, W. B., Cox, A. V., Lewellyn, P. G., Pickton, C. A. G., and Walters, R., 1982, A geologic time scale: Cambridge, Cambridge University Press, 131p.

Hatcher, R. D., 1990, Structural Geology: Principle, Concepts, and Problems: Fractures and faults, Merrill Publishing Company, Columbus, Ohio, p. 141-161.

Henbest, L.G., 1956, Foraminifera correlation of the Tensleep Sandstone of Pennsylvanian stage in Wyoming: Wyoming Geological Association, 11th Annual Field Conference Guidebook, p.58-63.

Hills, F. A., and Houston, R.S., 1979, Early Proterozoic tectonics of the Rocky Mountains, North America: University of Wyoming Contributions to Geology, v.17, p. 89-109.

Historical Wyoming Tidbits, Geologic History
http://www.wyomingbnb-ranchrec.com/History.Geologic.html

Hoare, R. D., and Burgess, J. D., 1960, Fauna from Tensleep Sandstone in Wyoming: Journal of Paleontology, v. 34, p. 711-716.

Hodgson, R. H., 1965, Genetic and geometric relations between structures in basement and overlying sedimentary rocks, with examples from Colorado Plateau and Wyoming: AAPG Bulletin, v.49, p. 935-949.

Hoppin, R. A., 1961, Precambrian rocks and their relationship to Laramide structure along the east flank of the Bighorn Mountains near Buffalo, Wyoming: GSA Bulletin, v. 72, p. 351-368.

Hoppin, R. A., 1974, Lineaments and their role in tectonics of central Rocky Mountains: AAPG Bulletin, v. 48, p. 2260-2273.

Hoppin, R. A., 1981, Review and synthesis of the tectonic lineaments of the world: A preliminary report: Proceedings of the Third International Conference on Basement Tectonics, p. 11-28.

Hoppin, R. A., J. C. Palmquist, and L. O. Williams, 1965, Control of Precambrian basement structure on the location of the Tensleep-Beaver Creek fault , Big Horn Mountains, Wyoming: Journal of Geology, v. 73, p. 189-195.

Hoppin, R. A., and Jennings, T. V., 1971, Cenozoic tectonic elements, Bighorn Mountain region, Wyoming-Montana: 23rd Annual Field Conference Guidebook, Wyoming Geological Association, p.39-47.

Hodgson, R. A., 1965, Genetic and geometric relations between structures in basement and overlying sedimentary rocks with examples from Colorado Plateau and Wyoming: AAPG Bulletin, v. 49, p. 935-949.

Hurley, N. F., Aviantara, A. A., and Kerr, D. R., 2000, Structural and stratigraphic compartments in a horizontal well drilled in the eolian Tensleep Sandstone, Byron field, Wyoming: AAPG memoir, in press.

Hurst, A., and Goggin, D., 1995, Probe permeametry: An overview and bibliography: AAPG Bulletin, v. 79, p.473-473.

Iverson, W. P., Dunn, T. L., and Ajdari, I., 1996, Relative permeability anisotropy measurements in Tensleep sandstone: SPE 35435, SPE/DOE 10th Symposium on Improved Oil Recovery.

Keefer, W. R., and Van Lieu, J. A., 1966, Paleozoic formations in the Wind River basin, Wyoming: U.S.G.S. Professional Paper 495-B, 60 p.

Kerr, D. R., 1989, Sedimentology and stratigraphy of Pennsylvanian and lower Permian strata (upper Amsden Formation and Tensleep Sandstone) in north-central Wyoming: Unpublished Ph.D. Thesis, University of Wisconsin-Madison, 381 p.

Kerr, D. R., Wheeler, D. M., Rittersbacher, D. J., and Horn, J. C., 1986, Stratigraphy and sedimentology of the Tensleep Sandstone (Pennsylvanian and Permian), Bighorn Mountains, Wyoming: Earth Science Bulletin, WGA, v. 19, part 2, p. 61-77.

Kerr, D. R., and Dott, R. H., Jr., 1988, Eolian dune types preserved in the Tensleep Sandstone (Pennyslvanian – Permian), north-central Wyoming: Sedimentary Geology, v. 56, no. 1-4, p. 383-402.

Kocurek, G. A., 1996, Desert eolian systems: *in* Reading, H. G., ed., Sedimentery environments: processes, facies and stratigraphy: Blackwell Science Ltd., p. 125-153.

Kulander, B.R., Barton, C.C., and Dean, S.L., 1979, The application of fractography to core and outcrop fracture investigations: Morgontown, West Virginia, DOE METC/SP-79/3, 174p.

Lapointe, P.R., 1980, Analysis of the special variation in rock mass properties through geostatistics, 21st U.S. Symposium on Rock Mechanics.

Limnological research center, http://lrc.geo.umn.edu/

Lindquist, S. J., 1988, Practical chracterization of the eolian reservoirs for development, Nugget Sandstone, Utah-Wyoming thrust belt: Sedimentary Geology, v. 56, p. 315-339.

Lyons, P. L., and O'Hara, W.O., 1982, Gravity anomaly map of the United States: Soc. Expl. Geophysicists.

Mankiewicz, D., and Steidtmann, J. R., 1979, Depositional environments and diagenesis of the Tensleep Sandstone, eastern Bighorn basin, Wyoming: SEPM Special Publication 26, p. 319-336.

Marrett, R., 1996, Aggregate properties of fracture populations: Journal of Structural Geology, v. 18, p. 169-178.

Morgan, J. T., Cordiner, F. S., and Livingston, A. R., 1978, Tensleep reservoir, Oregon Basin field, Wyoming: AAPG Bulletin, v. 62, p. 609-632.

Nasa, http://daac.gsfc.nasa.gov/DAAC_DOCS/geomorphology/GEO_2/GEO_PLATE_T-8.HTML

Nelson, R. A., 2001, Geologic Analysis of Naturally Fractured Reservoirs; Gulf Professional Publishing, Butterworth Heinemann, Boston, Second Edition, 332p.

Oduolowu, A., 1976, A case study of the recovable hydrocarbon volumes for the Minnelusa and Muddy sands, Powder River Basin, Wyoming:

Opdyke, N. D., and Runcorn, S. K., 1960, Wind direction in the Western United States in the Late Paleozoic: GSA Bulletin, v.71, p. 367-381.

Peterson, J. A., 1990, Petroleum potential outlined for northern Rockies, Great Plains: Oil and Gas Journal, v. 88, July 30, p. 103-110.

Rhodes, F. H. T., 1963, Conodonts from the topmost Tensleep Sandstone of the eastern bighorn Mountains, Wyoming, Journal of Paleontology, v. 37, p. 401-408.

Rittersbacher, D. J., 1985, Facies relationships of the Tensleep Sandstone and Minnelusa Formation, western Powder River basin, Johnson County, Wyoming: Unpublished MS Thesis, Colorado School of Mines, Golden, CO.

Sando, W. J., Gordon, M. Jr., and Dutro, J. T., Jr., 1975, Stratigraphy and geologic history of the Amsden Formation of Wyoming: United States Geological Survey Professional Paper 848-A, A83p.

Shebl, M. A., 1995, The impact of reservoir heterogeneity on fluid flow in the Tensleep Sandstone of the Bighorn Basin: 1995 Field Conference Guidebook, Wyoming Geological Association, p. 343-359.

Sheldon, R. P., 1967, Long distance migration of oil in Wyoming: The Mountain Geologist, v. 4, p. 53-65.

Snoke, A. W., 1997, Geologic history of Wyoming within the tectonic framework of the North American Cordillera: Wyoming State Geological Survey Public Information Circular 38, p. 1-52.

Suppe, J., 1985, Principles of structural geology: Prentice Hall, Eaglewood Cliffs, N.J., 437p.

Stone, D. S., 1967, Theory of Paleozoic oil and gas accumulation in the Bighorn basin, Wyoming: AAPG Bulletin, v. 51, p. 2056-2114.

Tanean, H., 1991, Multi scale reservoir characteristics of the Tensleep Formation, South Casper Creek field, Natrona County, Wyoming: Unpublished MS Thesis, Colorado School of Mines, Golden, 372p.

Todd, T. W., 1964, Petrology of Pennsylvanian rocks, Bighorn basin, Wyoming: AAPG Bulletin, v. 48, p.1063-1090.

USGS, 2000, USGS digital elevation model data:
http://edc.usgs.gov/glis/hyper/guide/usgs_dem

USGS, Rocky Mountain System
http://www.agd.nps.gov/grd/usgsnps/province/rockymtn.html

Van Eysinga, F. W. B., compiler, 1975, Geologic time table, Amsterdam, Elsevier, 1p.

Vealey, S., 1991, Reservoir characterization and heterogeneity of the Pennsylvanian Tensleep Sandstone at Alcova anticline, Natrona County, Wyoming: Unpublished Master's Thesis, Colorado School of Mines, Golden, CO, 181 p.

Verville, G. J., 1957, Wolfcampian fusulinids from the Tensleep sandstone in the Big Horn Mountains, Wyoming: Journal of Paleontology, v. 31, p.349-352.

Wilson, C. W., Jr., 1938, Geology of Nye-Bowler Lineament, Stillwater and Carbon Counties, Montana: AAPG Bulletin, v. 20, p. 1161-1188.

APPENDIX A

Scanline Data

ABBREVIATIONS

B: Bed

C: Calcite

Ft: Foot

GF: Grain Flow

O: Outcrop

R: Rock

SL: Scanline

T: T-junction

WR: Wind Ripple

Scan Line (SL) 1
Date 5/30/2000
Latitude 294118.676
Longitute 4916347.286
Orientation of SL N60W
Distance from fault (ft) 300
Total length of SL (ft) 24 1/2

								Fracture Termination			
Fracture No	**Facies**	**Distance from NW end of SL**	**Strike/Dip**	**Right hand rule**	**Dip direction/ Dip**	**Length to the NE (ft)**	**Length to the SW(ft)**	**To the NE**	**To the SW**	**Fracture Filling**	**Fracture Set**
A	Grain fall (GF)	6 1/4	N40E 82NW	220 82	310 82	14 1/2	4	Outcrop (O)	Outcrop	Calcite	Set 1
B	Grain fall (GF)	6 3/4	N40E 84NW	220 84	310 82	18 1/2	4 1/4	Outcrop	Outcrop	Calcite	Set 1
C	Grain fall (GF)	7 3/4	N46E 81NW	226 81	316 81	3 3/4	5 1/4	T junction (T)	Outcrop	Calcite	Set 1
D	Grain fall (GF)	8 1/2	N41E 60NW	221 60	311 60	30	3 1/4	Outcrop	Outcrop	Calcite	Set 1
F	Grain fall (GF)	28 1/3	N45E 80NW	225 80	315 80	20	3 1/4	Bed (B)	Bed	Calcite	Set 1

Strikes and dips around scanline 1

Strikes/Dips	**Right hand rule**
N51E 65NW	231 65
N17E 53NW	197 53
N22E 50NW	202 50
N25E 85NW	205 85
N40E 88NW	220 88
N33E 80NW	213 80
N54E 81NW	234 81
N40E 88NW	220 88
N75W 74SW	105 74
N20W 80SW	160 80
N35W 85SW	145 85
N85E 84NW	265 84
N10W 75SW	170 75
N6W 86NE	354 86
E-W 85N	270 85
N35W 85SW	145 85

Scan Line (SL) 2
Date 5/30/2000
Latitude 294106.736
Longitute 4916353.513
Orientation of SL E-W
Distance from fault (ft) 300
Total length of SL (ft) 35

Fracture No	Facies	Distance from W end of SL (ft)	Strike/Dip	Right hand rule	Dip direction/ Dip	Length to the N (ft)	Length to the S (ft)	Fracture Termination			
								To the N	To the S	Fracture Filling	Fracture Set
A	Both (GR,WR)	8 1/4	N10E 83SE	10 83	100 83	9 1/2	6 2/3	Bed(B)	Bed	Open	
B	Wind Ripple(WR)	8 1/2	N46E 85NW	226 85	316 85	9 2/3	13	Rock (R)	Outcrop(O)	Calcite	Set 1
C	Wind Ripple(WR)	17 1/2	N-S 78E	0 78	90 78	2 1/3	5 1/3	Rock	Rock	Open	Set 5
D	Wind Ripple(WR)	20	N40E 77SE	40 77	130 77	5 1/4	4 1/2	Rock	Rock	Calcite	Set 1
E	Wind Ripple(WR)	27 3/4	N6E 87SE	6 87	96 87	6 1/2	1	Bed	Rock	Open	Set 5
F	Both (GR,WR)	31 1/4	N-S 80E	0 80	90 80	15	3	Bed	Bed	Calcite	Set 5

Strikes and dips around scanline 2

Strikes/Dips	Right hand rule
N27E 83NW	207 83
N85W 90	95 90
N17E 88NW	197 88
N65E 62NW	245 62
N57W 40SW	123 40
N15E 86NW	195 86
N9E 86NW	189 86
N30E 87NW	210 87
N55E 83NW	235 83
N70W 84SW	110 84
N35E 79NW	215 79
N40E 35NW	220 35
N80E 72NW	260 72
N40E 70NW	220 70
N51W 65NE	309 65

Scan Line (SL) 3
Date 5/31/2000
Latitude 295401.277
Longitute 4916286.234
Orientation of SL N50W
Distance from fault (ft) 400
Scanline length (ft) 27

Fracture No	Facies	Distance from NW end of SL	Strike/Dip	Right hand rule	Dip direction/ Dip	Length to the NE (ft)	Length to the SW(ft)	Fracture Termination		Fracture Filling	Fracture Set
								To the NE	To the SW		
A	WR	10 1/2	N45E 70NW	225 70	315 70	20	13	Rock	O	Calcite	Set 1
B	WR	23	N65E 85SE	65 85	155 85	2	5	Rock	R	Calcite	Set 3
C	WR	24 3/4	N65E 82SE	65 82	155 85	2	2 1/2	Outcrop	O	Calcite	Set 3
D	WR	25	N64E 78SE	64 78	154 78	2	2 1/2	Outcrop	O	Calcite	Set 3
E	WR	25 1/3	N68E 79NW	248 79	338 79	1 2/3	3	Outcrop	O	Calcite	Set 3
F	WR	27	N67E 85NW	247 85	337 85	3	3 1/3	Outcrop	O	Calcite	Set 3

Strikes and dips around scanline 3

Strikes/Dips	Right hand rule
N25E 81SE	25 81
N20E 62SE	20 62
E-W 80N	270 80
N55W 83SW	125 83
N15E 46SE	15 46
N60E 79NW	240 79
N40E 86NW	220 86
N50W 66SW	130 66
N53W 69SW	127 69
N75W 77SW	105 77
NS 85W	180 85
N20E 80SE	20 80
N30W 81NE	330 81
N10W 83NE	350 83
N20E 66SE	20 66
NS 75W	180 75
NS 90	0 90

Scan Line (SL) 4
Date 5/31/2000
Latitude 295398.864
Longitute 4916287.721
Orientation of SL N35E
Distance from fault (ft) 400
Total length of SL (ft) 31

Frac #	Facies	Distance from SW end of SL (ft)	Strike/Dip	Right hand rule	Dip direction/ dip	Length to the NW (ft)	Length to the SE (ft)	Fracture Termination			Fracture Set
								To the NW	To the SE	Fracture Filling	
			N50W 86SW	140 86	230 86						
A- 20 fractures	WR	in 5 1/3	N5E 85NW	185 85	275 85			Outcrop	R	Open	Set 5
B	WR	8 1/4	N52W 67NE	308 67	38 67	1 2/3	12	Rock	R	Open	Set 6
C	WR	8 1/2	N53W 65NE	307 65	37 65	1 2/3	10 1/4	Rock	R	Open	Set 6
D- 6 Fractures	WR	12 3/4-15 1/4	N60W 85NE	300 85	30 85	2	3 3/4	Rock	R	Open	Set 6
E	WR	23 1/2	N23W 65SW	157 65	247 65	1 2/3	5 1/2	Bed	O	Open	
F	WR	25	N20W 38SW	160 38	250 38	1 1/2	22 1/4	Bed	O	Open	
G	WR	29	E-W 87S	90 87	180 87	3	10 1/4	Bed	R	Open	Set 4

Strikes and dips around scanline 4

Strikes/Dips	Right hand rule
N65E 63SE	65 63
N60W 81SW	120 81
N47E 77NW	227 77
N55W 81SW	125 81
N40W 82NE	320 82
NS 87W	180 87
N60W 63SW	120 63
NS 59W	180 59
N5W 86SW	175 86
N40W 90	140 90
N4W 85NE	356 85
N6W 77SW	174 77
N27W 75SW	153 75
N10W 83NE	350 83
N65E 85SE	65 85
N67E 77SE	67 77
N52E 73SE	52 73

Scan Line (SL) 5
Date 6/1/2000
Latitude 295558.137
Longitute 4916376.013
Orientation of SL N50W
Distance from fault (ft) 400
Total length of SL (ft) 16 1/2

Fracture No	Facies	Distance from NW end of SL	Strike/Dip	Right hand rule	Dip direction/ Dip	Length to the NE (ft)	Length to the SW(ft)	Fracture Termination		Fracture Filling	Fracture Set
								To the NE	To the SW		
A	GF	1	N55E 58NW	235 58	325 58	3 3/4	10 3/4	Outcrop	O	Calcite	
B	GF	2 1/4	N52E 47NW	232 47	322 47	3 1/2	9 1/2	Outcrop	O	Calcite	Set 1
C	GF	3 2/3	N40E 66NW	220 66	310 66	1/2	10 1/4	Rock	O	Calcite	Set 1
D	GF	7 3/4	N50E 70NW	230 70	320 70	6	7	Outcrop	O	Calcite	Set 1
E	GF	9 1/4	N10E 65NW	190 65	280 65	2 1/2	3 1/2	T junktion	T	Calcite	
F	GF	9 1/2	N23W 65NE	337 65	337 65	4	6	T junktion	O	Calcite	
G	GF	10 1/2	N50E 56NW	236 56	230 56	4	5	T junktion	O	Calcite	Set 1
H	GF	11 1/2	N28E 78SE	28 78	118 78	3/4	3 2/3	Rock	O	Calcite	Set 2
I	GF	12	N35E 78SE	35 78	125 78	6	4	Rock	O	Calcite	
J	GF	12 1/2	N50E 85SE	50 85	140 85	4	4	Rock	O	Calcite	Set 1
K	GF	12 3/4	N35E 86NW	215 86	305 86	8	3	Outcrop	O	Calcite	
L	GF	16	N40E 63NW	220 63	310 63	9	4	Outcrop	O	Calcite	Set 1
M	GF	16 1/3	N43E N48W	223 48	313 48	10	2	Outcrop	O	Calcite	Set 1

Strikes and dips around scanline 5

Strikes/Dips	Right hand rule
N80E / 86NW	260 86
N-S / 85W	180 85
E-W / 81S	90 81
N80E / 77SE	80 77
N60W / 75SW	120 75
N-S / 81E	0 81
N63E / 87SE	63 87
N40E / 85SE	40 85
N84W / 84NE	276 84
E-W / 81N	270 81
N84E / 83SE	84 83
N-S / 76W	180 76

Scan Line (SL) 6
Date 6/1/2000
Latitude 295556.748
Longitute 4916378.373
Orientation of SL N80W
Distance from the fault (ft) 400
Total Lenth of the SL (ft) 17

								Fracture Termination			
Fracture No	**Facies**	**Distance from NW end of SL**	**Strike/Dip**	**Right hand rule**	**Dip direction/ Dip**	**Length to the NE (ft)**	**Length to the SW(ft)**	**To the NE**	**To the SW**	**Fracture Filling**	**Fracture Set**
26 fractures	GF	In all length	N15W 80-90SW	165 65-80	255 65-80	Between 1	Between 3-5	19O 7R	23R 3T	Calcite	
4 fractures	GF	In all length	N30E 75SE	30 75	120 75	3	3	R	R	Calcite	

Strikes and dips around scanline 6

Strikes/Dips	**Right hand rule**
N-S / 71W	180 71
N55E / 68SE	55 68
N80E / 63SE	80 63
N80E / 86NW	260 86
N60E / 63NW	240 63
N-S / 69W	180 69
N10E / 87NW	190 87
N5E / 86NW	185 86
N30E / 80NW	210 80
N10E / 83NW	190 83
N50W / 83NE	310 83
N30W / 85NE	330 85
N-S / 84W	180 84
N50E / 76NW	230 76
N30E / 78NW	210 78
N24E / 84NW	204 84
N7W / 50NE	353 50
N25E / 63NW	205 63

Scan Line (SL) 7
Date 6/1/2000
Latitude 294927.846
Longitute 4916399.888
Orientation of SL E-W
Distance from fault (ft) 300
Total length of SL (ft) 18

Fracture No	Facies	Distance from W end of SL (ft)	Strike/Dip	Right hand rule	Dip direction/ Dip	Length to the N (ft)	Length to the S (ft)	Fracture Termination			
								To the N	To the S	Fracture Filling	Fracture Set
A	GF	1/4	N49E 73NW	229 73	319 73	5	5	Rock	T	Calcite	Set 1
B	GF	1/2	N57E 75NW	237 75	327 75	4	5	Rock	T	Calcite	
C	GF	1	N10E 71NW	190 71	280 71	6	11	Rock	R	Calcite	Set 5
D	GF	1 1/4	N53E / 76NW	233 76	323 76	5	4	Rock	T	Calcite	Set 1
E	GF	1 1/2	N48E / 75NW	228 75	318 75	1	15	Rock	O	Calcite	Set 1
F	GF	4 1/3	N57E / 81NW	237 81	327 81	8	9	Rock	R	Calcite	
G	GF	4 1/2	N30E / 80NW	210 80	300 80	1 3/4	1 1/2	T junktion	T	Calcite	
H	GF	5 3/4	N57E / 73NW	237 73	327 73	8	2 1/2	Rock	T	Calcite	
I	GF	6 1/3	N49E / 69NW	229 69	319 69	7	16	Rock	O	Calcite	Set 1
J	GF	6 1/3	N22E / 81NW	202 81	292 81	15	2 1/2	Bed	O	Calcite	Set 2
K	GF	9	N10E / 77NW	190 77	280 77	1 3/4	4	Rock	O	Calcite	Set 5
L	GF	10	N45E / 71NW	225 71	315 71	10	9	Rock	O	Calcite	Set 1
M	GF	11 2/3	N7E / 65NW	187 65	277 65	6	8	Bed	O	Open	Set 5
N	GF	14 1/4	N-S / 81W	180 81	270 81	4	7	Bed	O	Open	Set 5
O	GF	16 1/2	N8E / 83NW	188 83	278 83	10	9	Outcrop	O	Open	Set 5
P	GF	17 1/3	N-S / 80W	180 80	270 80	5	4	Outcrop	O	Open	Set 5

Strikes and dips around scanline 7

Strikes/Dips	Right hand rule
N15E / 87NW	195 87
N5E / 72NW	185 72
N40E / 68NW	220 68
N28W / 87NE	332 87
N-S / 84E	0 84
220N / 88W	220 88
N22W / 46SW	158 46
E-W / 81S	180 81
N20E / 83NW	200 83
N29E / 85NW	209 85
N55E / 87NW	235 87
N82E / 25NW	262 25
N10W / 81SW	170 81

Scan Line	8
Date	6/1/2000
Latitude	294920.833
Longitute	4916400.184
Orientation of SL	N60E
Distance from fault (ft)	300
Total length of SL (ft)	19

								Fracture Termination			
Frac #	**Facies**	**Distance from SW end of SL (ft)**	**Strike/Dip**	**Right hand rule**	**Dip direction/ dip**	**Length to the NW (ft)**	**Length to the SE (ft)**	**To the NW**	**To the SE**	**Fracture Filling**	**Fracture Set**
A	GF	3	N-S / 81W	180 81	270 81	5	1/2	Rock	R	Open	Set 5
B	GF	6 1/2	N-S / 85W	180 85	270 81	1	2	Rock	R	Open	Set 5
C	GF	15 1/2	N-S / 35W	180 35	270 35	2 1/4	9 1/4	Bed	R	Open	Set 5
D	GF	18 1/4	N20W / 33SW	160 33	250 33	9	11	Bed	O	Open	

Strikes and dips around scanline 8

Strikes/Dips	**Right hand rule**
N80E / 40NW	250 40
N30W / 30NE	330 30
N55E / 70NW	235 70
N75E / 77SE	75 77
N33E / 84SE	33 84
N15E / 87NW	195 87
N45E / 35SE	45 35
N20E / 75NW	200 75
N62W / 84NE	298 84
N35E / 77NW	215 77
N25E / 85SE	25 85
N33E / 77NW	213 77
N20E / 65NW	200 65
N40E / 83NW	220 83
N36E / 82NW	216 82
N28E / 83NW	208 83
N36E / 84NW	216 84
N18E / 87NW	198 87
N44E / 81NW	224 81
N25W / 85NE	335 85

Scan Line 9
Date 6/3/2000
Latitude 295614.099
Longitute 4915476.536
Orientation of SL N84W
Distance from the fault (ft) 1700
Total length of the SL (ft) 36 3/4

								Fracture Termination			
Fracture No	**Facies**	**Distance from NW end of SL**	**Strike/Dip**	**Right hand rule**	**Dip direction/ Dip**	**Length to the NE (ft)**	**Length to the SW(ft)**	**To the NE**	**To the SW**	**Fracture Filling**	**Fracture Set**
A	WR	11 3/4	N33E / 87NW	213 87	303 87	6	7	Bed	O	Open	
B	WR	16 1/2	N45W / 74SW	135 74	255 74	2 1/2	2 1/4	Rock	O	Open	
C	WR	20 1/2	N-S / 82W	180 82	270 82	6	1/2	Rock	T	Open	Set 5
D	WR	23 1/2	N49W / 87SW	131 87	200 87	3 1/2	1	Rock	R	Open	Set 6
E	WR	33 1/4	N55E / 59NW	125 59	325 59	5	6	Rock	O	Open	Set 6

Strikes and dips around scanline 9

Strikes/Dips	**Right hand rule**
N50E / 81NW	230 81
N15E / 77NW	195 77
NS / 85W	180 85
N6E / 87SE	6 87
N15W / 83NE	345 83
N86E / 87NW	266 87
N85W / 85SW	95 85
N27E / 87NW	207 87
N30W / 79SW	150 79
N10E / 85SE	10 85
N55E / 84SE	55 84
N80W / 87NE	280 87
N25E / 81SE	25 81
N73E / 86NW	253 86
N70E / 87NW	250 87
N45W / 54SE	135 54
N49W / 64SE	131 64

Scan Line (SL) 10
Date 6/3/2000
Latitude 295614.897
Longitute 4915484.948
Orientation of SL N20E
Distance from the fault (ft) 1700
Total length of the SL (ft) 36 1/3

								Fracture Termination			
Frac #	**Facies**	**Distance from SW end of SL (ft)**	**Strike/Dip**	**Right hand rule**	**Dip direction/ dip**	**Length to the NW (ft)**	**Length to the SE (ft)**	**To the NW**	**To the SE**	**Fracture Filling**	**Fracture Set**
A	WR	3	N85E / 83SE	85 83	355 83	1 1/2	3	Bed	O	Open	Set 4
B	WR	6 3/4	N66W /87NE	294 87	24 87	1	4	Rock	R	Open	Set 6
C	WR	9 1/4	N40W / 83NE	320 83	50 83	1 3/4	3 3/4	Bed	O	Open	
D	WR	12 1/3	E-W / 87N	270 87	0 87	4 1/4	2 1/4	Rock	O	Open	Set 4
E	WR	14 1/2	N51W / 86NE	309 86	39 86	2	3 3/4	Bed	B	Open	Set 6
F	WR	17 1/2	N45E / 79SE	45 79	135 79	1 1/2	3 1/4	Rock	T	Open	Set 1
G	WR	19 1/4	E-W / 78N	270 78	0 78	1	8	Outcrop	O	Open	Set 4
H	WR	21 2/3	N63W / 86NE	297 86	27 86	1/2	3	Outcrop	O	Open	Set 6
I	WR	27 3/4	N55W /73NE	305 73	35 73	1 1/4	5 1/4	Outcrop	O	Open	Set 6
J	WR	34 1/2	N47E / 84SE	47 81	237 81	1 1/3	3 1/3	Rock	O	Open	Set 1

Strikes and dips around scanline 10

Strikes/Dips	**Right hand rule**
N33W / 79SE	147 79
N19W / 59NE	341 59
N25E / 87NW	205 87
N77W / 83SW	103 83
E-W / 77S	90 77
N55E / 33SE	55 33
E-W / 79S	90 79
E-W / 85S	90 85
N77W / 84SW	103 84
N71W / 86SW	109 86
N-S / 44E	0 44
N60E / 80SE	60 80
N4E / 69SE	4 69
N10E / 77SE	10 77
N11E / 86SE	11 86
E-W / 81S	90 81

Scan Line (SL) 11
Date 6/3/2000
Latitude 295552.472
Longitute 4915594.755
Orientation of SL N10E
Distance from fault (ft) 1400
Total length of SL (ft) 26 1/4

Frac #	Facies	Distance from SW end of SL (ft)	Strike/Dip	Right hand rule	Dip direction/ dip	Length to the NW (ft)	Length to the SE (ft)	Fracture Termination			
								To the NW	To the SE	Fracture Filling	Fracture Set
A	GF	3 3/4	N35W / 87SW	145 87	235 87	1 1/4	2 1/4	Rock	R	Open	
B	GF	12 1/4	N35W / 78SW	145 78	235 78	1 1/4	2 1/4	Rock	R	Calcite	
C	GF	13	N10E / 81SE	10 81	100 81	3	2 1/4	Rock	R	Calcite	
D	GF	14 3/4	N47E / 67SE	47 67	137 67	1	3	Rock	R	Calcite	Set 1
E	GF	15	N66W / 85SW	114 85	204 85	5	1	Outcrop	T	Open	Set 6
F	GF	17	N50W / 64SW	130 64	220 64	1	2 1/4	Rock	R	Open	Set 6
G	GF	24 3/4	N50W / 76SW	130 76	220 76	1	2 1/3	Rock	R	Open	Set 6

Strikes and dips around scanline 11

Strikes/Dips	Right hand rule
N70W / 58NE	290 58
N19W / 64NE	341 58
N12W / 57NE	348 57
N24W / 74NE	338 74
N50W / 86NE	310 86
N60W / 85NE	300 85
N33W / 81NE	327 81
N41W / 73NE	319 73
N80E / 84SE	80 84
N65E / 81SE	65 81
N37E / 88SE	37 88
N45W / 74NE	315 74
N11W / 84NE	349 84
N27W / 73NE	333 73
N30W / 72NE	330 72
N-S / 64E	0 64

Scan Line (SL)	12
Date	6/3/2000
Latitude	295552.867
Longitute	4915603.443
Orientation of SL	N75E
Distance from fault (ft)	1400
Total length of SL (ft)	23

								Fracture Termination			
Frac #	**Facies**	**Distance from SW end of SL (ft)**	**Strike/Dip**	**Right hand rule**	**Dip direction/ dip**	**Length to the NW (ft)**	**Length to the SE (ft)**	**To the NW**	**To the SE**	**Fracture Filling**	**Fracture Set**
A	WR	3 1/4	N29W / 81NE	331 81	61 81	1	3	R	B	Open	
B	WR	6 1/3	N28W / 69NE	332 69	62 69	1	2 3/4	R	B	Open	
C	WR	9 2/3	N25W / 70NE	335 70	65 70	1	2 1/2	R	B	Open	
D	WR	13 1/2	N15W / 90	165 90	255 90	1	4	R	B	Open	
E	WR	20	N33W / 81NE	327 81	57 81	1 3/4	5	B	B	Open	

Strikes and dips around scanline 12

Strikes/Dips	**Right hand rule**
N4W / 58NE	356 58
N20W / 84NE	340 84
N-S / 61E	0 61
N26W / 67NE	334 67
N15E / 90	15 90
N-S / 85E	0 85
N26W / 79NE	334 79
N15W / 84NE	345 84
N71E / 81SE	71 81
N78E / 82SE	78 82
N53W / 80NE	307 80
N10W / 79NE	350 79
N32E / 81NW	212 81
N63E / 83SE	63 83
N70E / 81SE	70 79
N76E / 82SE	76 82

Scan Line (SL) 13
Date 6/5/2000
Latitude 295521.174
Longitute 4916403.828
Orientation of SL N17W
Distance from fault (ft) 300
Total length of SL (ft) 30 3/4

Fracture No	Facies	Distance from NW end of SL (ft)	Strike/Dip	Right hand rule	Dip direction/ Dip	Length to the NE (ft)	Length to the SW(ft)	Fracture Termination		Fracture Filling	Fracture Set
								To the NE	To the SW		
A	WR	9 3/4	N60W / 81NE	300 81	30 81	2	1 1/4	R	Bed	Open	Set 6
B	WR	16 1/3	N59W / 78NE	301 78	31 78	3	3/4	R	B	Open	Set 6
C	WR	21	N56W / 84NE	304 84	34 84	4 1/2	3/4	T	T	Open	Set 6
D	WR	24 1/3	N83W / 79SW	97 79	187 79	15	2	O	O	Open	
E	WR	27	E-W / 86N	270 86	0 86	3	1	O	B	Open	Set 4
F	WR	30 1/4	N80W / 68NE	280 68	10 68	2	1	R	O	Open	

Strikes and dips around scanline 13

Strikes/Dips	Right hand rule
E-W / 87N	270 87
E-W / 86N	270 86
N22W / 72NE	338 72
N10W / 83NE	350 83
N49W / 85NE	311 85
N25W / 90	155 90
N42E / 87SE	42 87
N49E / 86SE	49 86
N37E / 79SE	37 79
N23W / 90	157 90
N15E / 87SE	15 87
N45E / 86SE	45 86
N63E / 81SE	63 81
N4W / 90	176 90
N30E / 71NW	210 71
N10W / 74SW	170 74
N12E / 79NW	192 79

Scan Line (SL) 14
Date 6/3/2000
Latitude 295538.088
Longitute 4916381.699
Orientation of SL N35W
Distance from fault (ft) 300
Total length of SL (ft) 30 3/4

Fracture No	Facies	Distance from NW end of SL (ft)	Strike/Dip	Right hand rule	Dip direction/ Dip	Length to the NE (ft)	Length to the SW(ft)	Fracture Termination		Fracture Filling	Fracture Set
								To the NE	To the SW		
A	WR	1/2	N81W / 87NE	279 87	9 87	2 1/4	1	R	O	Calcite	Set 4
B	WR	2 1/4	N60E / 86NW	240 86	330 86	1/2	3 1/4	B	R	Open	
C	WR	6	N85W / 86NE	275 86	5 86	4	15	O	O	Open	Set 4
D	WR	15	N80E / 74SE	80 74	170 74	3	3	O	O	Open	
E	WR	16 1/2	E-W / 75S	90 75	180 75	2	20	O	O	Open	Set 4
F	WR	18 1/4	E-W / 76S	90 76	180 76	2 1/2	20	O	O	Open	Set 4
G	WR	19	N78W / 83SW	102 83	192 83	1 1/4	2	O	T	Open	Set 4
H	WR	20 3/4	E-W / 90	90 90	180 90	2 1/2	6	O	O	Open	Set 4
I	WR	24 1/2	N80W / 90	100 90	190 90	4	1	R	R	Open	Set 4
J	WR	25 1/2	N80W / 90	100 90	190 90	7	5	R	R	Open	Set 4

Strikes and dips around scanline 14

Strikes/Dips	Right hand rule
N55E / 66SE	55 66
N52E / 81SE	52 81
N38E / 78SE	38 78
N47E / 71SE	47 71
N12E / 66SE	12 66
N5E / 44SE	5 44
N63E / 50SE	63 50
N61E / 79SE	61 79
N38E / 80SE	38 80
N23E / 62SE	23 62
N-S / 66E	0 66
N56E / 83SE	56 83
N48W / 77NE	312 77

Scan Line (SL)	15
Date	6/6/2000
Latitude	295329.011
Longitute	4916250.747
Orientation of SL	N30E
Distance from fault (ft)	600
Total length of SL (ft)	34 1/4

								Fracture Termination			
Frac #	**Facies**	**Distance from SW end of SL (ft)**	**Strike/Dip**	**Right hand rule**	**Dip direction/ dip**	**Length to the NW (ft)**	**Length to the SE (ft)**	**To the NW**	**To the SE**	**Fracture Filling**	**Fracture Set**
A	WR	2 3/4	N37W / 81NE	323 81	53 81	1	2	B	B	Open	
B	WR	6 1/3	N41W / 85NE	319 85	49 85	1 1/4	3	R	R	Open	Set 6
C	WR	10 1/2	N40W / 74NE	320 74	50 74	1 1/4	8	R	B	Open	Set 6
D	WR	16 1/2	N40W / 79NE	320 75	50 79	3	3 1/4	B	R	Open	Set 6
E	WR	26 1/2	N73W / 85NE	287 85	17 85	3 1/3	3 3/4	R	R	Open	
F	WR	32 1/4	N45E / 71SE	45 71	135 71	1 1/4	3	B	R	Open	Set 1

Strikes and dips around scanline 15

Strikes/Dips	**Right hand rule**
E-W / 84N	270 84
N49W / 84NE	311 84
N12E / 84SE	12 84
N15E / 66SE	15 66
N11E / 79SE	11 79
N15E / 81SE	15 81
N13E / 78SE	13 78
N35E / 71NW	215 71
N85E / 81NW	265 81
N-S / 87E	0 87
N10W / 83NE	350 83
N48W / 65NE	312 65
N10W / 63NE	350 63
N18W / 61NE	342 61
N49E / 69NW	229 69

Scan Line (SL)	16
Date	6/6/2000
Latitude	295413.947
Longitute	4916357.434
Orientation of SL	N78E
Distance from fault (ft)	600
Total length of SL (ft)	23

								Fracture Termination			
Frac #	**Facies**	**Distance from SW end of SL (ft)**	**Strike/Dip**	**Right hand rule**	**Dip direction/ dip**	**Length to the NW (ft)**	**Length to the SE (ft)**	**To the NW**	**To the SE**	**Fracture Filling**	**Fracture Set**
A	WR	8	N7E / 87SE	7 87	97 87	1 1/4	40	O	R	Open	Set 5
B	WR	18	N1W / 58NE	359 58	89 58	2 1/4	2 1/4	O	R	Open	Set 5
C	WR	23	N-S / 81W	0 81	90 81	2 1/2	7 1/4	R	O	Open	Set 5

Strikes and dips around scanline 16

Strikes/Dips	**Right hand rule**
N50E / 74NW	230 74
N38E / 87NW	218 87
N46E / 38SE	46 38
N48E / 38SE	48 38
N52W / 79SW	128 79
N16W / 71NE	344 71
N28W / 84NE	332 84
N63E / 56NW	243 56
N75W / 69NE	285 69
N80E / 79SE	80 79
N51W / 71NE	309 71
N44W / 78NE	316 78
N10W / 81NE	350 81
N-S / 83E	0 83

Scan Line (SL) 17
Date 6/6/2000
Latitude 4916046.959
Longitute 1778.556
Orientation of SL N17W
Distance from fault (ft) 150
Total length of SL (ft) 30 1/4

Fracture No	Facies	Distance from NW end of SL (ft)	Strike/Dip	Right hand rule	Dip direction/ Dip	Length to the NE (ft)	Length to the SW(ft)	Fracture Termination			
								To the NE	To the SW	Fracture Filling	Fractue Set
A	WR	2 1/4	N48E / 71NW	228 71	318 71	1	2 1/4	B	B	Open	Set 1
B	WR	6 1/2	N54E / 61NW	234 61	324 61	1 3/4	7 1/2	R	R	Open	Set 1
C	WR	9 1/2	N48E / 61NW	228 61	318 61	2 1/4	5 3/4	B	R	Open	Set 1
D	WR	15 1/2	N45E / 90	45 90	135 90	1	2	R	R	Open	Set 1
E	WR	19 1/4	N48E / 90	48 90	138 90	1	2 3/4	R	R	Open	Set 1
F	WR	18 1/2	N48E / 90	48 90	138 90	1	3	B	B	Open	Set 1

Strikes and dips around scanline 17

Strikes/Dips	Right hand rule
N11W / 71SW	169 71
N63E / 81NW	243 81
N78E / 90	78 89
N81E / 87NW	261 87
N28W / 66NE	332 66
N75W / 81NE	285 81
N56W / 83SE	124 83
N76W / 83NE	284 83
N48E / 83NW	228 83
N-S / 90	0 90
N53E / 34NW	233 34
N33W / 90	147 89
N75W / 67NE	285 67
N50E / 90	50 90
N69W / 66NE	291 66
N73E / 83NW	253 83
N81E / 90	81 90
N35W / 74NE	325 74

Scan Line (SL) 18
Date 6/10/2000
Latitude 4916566.754
Longitute 1966.370
Orientation of SL N75W
Distance from fault (ft) 150
Total length of SL (ft) 24 1/2

Fracture No	Facies	Distance from NW end of SL (ft)	Strike/Dip	Right hand rule	Dip direction/ Dip	Length to the NE (ft)	Length to the SW(ft)	Fracture Termination			
								To the NE	To the SW	Fracture Filling	Fracture Set
A	WR	3 1/2	N44E / 81NW	224 81	314 81	1	10 1/4	O	O	Open	Set 1
B	WR	6 1/2	N50E / 83NW	230 83	320 83	1 1/4	6 1/3	O	O	Open	Set 1
C	WR	9 2/3	N47E / 87NW	227 87	317 87	1 1/4	3 1/3	R	O	Open	Set 1
D	WR	13 3/4	N75E / 81NW	255 81	345 81	1 1/2	4 1/4	R	O	Calcite	Set 3
E	WR	15 1/3	N47E / 86NW	227 86	317 86	1	7 1/4	R	O	Open	Set 1
F	WR	15 3/4	N64E / 87NW	244 87	334 87	1	6 1/2	O	R	Open	
G	WR	17 1/4	N70E / 88NW	250 88	340 88	1	13 1/2	O	O	Calcite	Set 3
H	WR	19 1/2	N38E / 85NW	218 85	308 85	2	5 1/4	O	O	Open	
I	WR	20 1/3	N50E / 88NW	230 88	320 88	1	5	O	O	Open	Set 1
J	WR	22	N51E / 87NW	231 87	321 87	1	5 1/4	O	O	Open	Set 1
K	WR	21 1/4	N47E / 85NW	227 85	317 85	1 1/4	4 1/2	O	O	Open	Set 1

Strikes and dips around scanline 18

Strikes/Dips	Right hand rule
N80W / 83NE	280 83
N15E / 79SE	15 79
N65W / 58NE	295 58
N73W / 66NE	287 66
N65W / 66NE	295 66
N55W / 68NE	305 68
N25W / 71NE	335 71
N70W / 54NE	290 54
N66E / 90	66 90
N10W / 81SW	170 81
N3W / 90	177 90
N3E / 90	3 90
N49E / 81NW	229 81
N65E / 80NW	245 80

Scan Line (SL) 19
Date 6/10/2000
Latitude 295329.098
Longitute 4916250.684
Orientation of SL N10E
Distance from fault (ft) 900
Total length of SL (ft) 29 3/4

Frac #	Facies	Distance from SW end of SL (ft)	Strike/Dip	Right hand rule	Dip direction/ dip	Length to the NW (ft)	Length to the SE (ft)	Fracture Termination			Fracture Set
								To the NW	To the SE	Fracture Filling	
A	WR	2 1/4	E-W / 81S	90 81	180 81	1	5	O	O	Open	Set 4
B	WR	2 3/4	N81W / 81SW	99 81	189 81	1	6	O	O	Open	Set 4
C	WR	4 3/4	N88W / 80SW	92 80	182 80	1 1/4	2 3/4	O	O	Open	Set 4
D	WR	5 3/4	N82W / 81SW	98 81	188 81	1 1/4	2 2/3	O	O	Open	
E	WR	6 3\4	N79W / 76SW	101 76	191 76	1 1/4	3	O	O	Open	
F	WR	7 1/4	N85W / 79SW	95 79	185 79	1 3/4	3	O	O	Open	Set 4
G	WR	7 1/2	E-W / 90	90 90	180 90	1	3	O	O	Open	Set 4
H	WR	9 1/3	N85W / 90	175 90	265 90	3	2 1/2	O	O	Open	Set 4
I	WR	11 3/4	N87W / 90	177 90	267 90	3	6	O	O	Open	Set 4
J	WR	24 1/2	N88W / 71SW	92 71	182 71	2	2	O	O	Open	Set 4
K	WR	251/3	N88W / 83SW	99 83	182 83	2	6	O	O	Open	Set 4
L	WR	26 1/2	N85W / 83SW	95 83	185 83	2	5	O	O	Open	Set 4

Strikes and dips around scanline 19

Strikes/Dips	Right hand rule
N35E / 74NW	215 74
N46E / 67NW	226 67
N73E / 59NW	253 59
N70E / 49NW	250 49
N58E / 66NW	238 66
N66E / 68NW	246 68
N58E / 56NW	238 56
N78E / 89NW	258 89
N48E / 85NW	228 85
N28E / 85NW	208 85
E-W / 48S	90 48
N13E / 66SE	13 66
N28E / 54SE	28 54

Scan Line (SL)	20
Date	6/10/2000
Latitude	295406.003
Longitute	4916262.896
Orientation of SL	N76E
Distance from fault (ft)	900
Total length of SL (ft)	22 3/4

								Fracture Termination			
Frac #	**Facies**	**Distance from SW end of SL (ft)**	**Strike/Dip**	**Right hand rule**	**Dip direction/ dip**	**Length to the NW (ft)**	**Length to the SE (ft)**	**To the NW**	**To the SE**	**Fracture Filling**	**Fracture Set**
A	GF	1	N43E / 81NW	223 81	313 81	9 3/4	2 3/4	R	O	Open	Set 1
B	GF	8 3/4	N4E / 84NW	184 84	274 84	6 1/2	5 1/2	R	O	Open	Set 4
C	GF	12 1/2	N45E / 86NW	225 86	315 86	8 1/2	6 3/4	T	T	Open	Set 1
D	GF	14	N20E / 85NW	200 85	290 85	2 1/4	4 1/2	R	O	Calcite	Set 2
E	GF	18 1/4	N44E / 84NW	224 84	314 84	3 3/4	8 1/2	R	O	Open	Set 1

Strikes and dips around scanline 20

Strikes/Dips	**Right hand rule**
N-S / 88W	180 88
N60E / 63NW	240 63
N81E / 52NW	261 52
N80E / 74NW	260 74
N73E / 72NW	253 72
N55E / 70NW	235 70
N66E / 79NW	246 79
N30W / 88NE	330 88
N18W / 79SW	162 79
N57W / 85NE	303 85
N60W / 83NE	300 83
N-S / 66W	180 66
N10E / 67NW	190 67
N15E / 56NW	195 56
N70E / 81NW	250 81

Strikes and dips in close range within 40 ft (12 m) of the Alkali fault

Strikes/Dips	Right hand rule	
N73E / 87NW	253 87	
N33E / 85SE	33 85	
N57E / 87NW	237 87	
N35E / 84NW	215 84	Their length is aproximately 1m and have calcite filling.
E-W / 85S	90 85	
N80E / 83SE	80 83	
N35E / 87SE	35 87	
N43E / 71SE	43 71	There are fractures aproximately parallel to each other. Therefore, this strike and dip represents 6 fractures, whose fracture spacing less than a feet.
N53E / 80SE	53 80	
N57E / 83SE	57 83	Calcite filled fractures.
N70E / 85SE	70 85	
N60E / 71NW	240 71	
N38E / 81SE	38 81	
N30E / 79SE	30 79	
N77E / 49SE	77 49	Calcite filled fractures.
N58E / 63NW	238 63	
N80E / 48NW	260 48	
N66E / 81NW	246 81	
N47E / 63NW	227 63	
N40E / 78NW	220 78	
N25E / 87NW	205 87	
N-S / 88W	180 88	Calcite filled fracture.
N28E / 66NW	208 46	
E-W / 46N	270 46	
N40E / 77SE	40 77	Calcite filled fracture.
N63E / 81SE	63 81	
N54E / 81NW	234 81	
N23W / 46NE	337 46	Calcite filled fracture.
N33E / 67NW	213 67	
N8E / 54SE	8 54	
N41E / 73NW	221 73	This strike and dip measurement for 11 calcite filled fractures whose spacing are between 7-20 cm.
N17E / 78NW	197 78	
N7E / 81NW	187 81	
N7W / 78SW	173 78	
N43E / 89	223 89	
N35E / 89NW	115 89	
N42E / 89NW	222 89	
N48E / 73NW	228 73	
N48E / 77NW	228 77	These calcite filled fractures have 1 cm aperture.

N68E / 66NW	248 66	
N31E / 89NW	211 89	
N77E / 69NW	257 69	
N35E / 74NW	254 74	
N46E / 67NW	226 67	
N73E / 59NW	253 59	
N70E / 49NW	250 49	
N58E / 66NW	238 66	
N66E / 68NW	246 68	
N58E / 56NW	238 56	
N78E / 89NW	258 89	
N48E / 85NW	228 85	
N28E / 85NW	208 85	
E-W / 48S	90 48	
N13E / 66SE	13 66	
N28E / 54SE	28 54	
N-S / 74W	180 74	
N27E / 60NW	207 60	This stike and dip for 9 calcite filled fractures whose aperture are between 0.5-1 cm. Their lengths are more than 10 m.
N10E / 66NW	190 66	
N14E / 81NW	194 81	
N21E / 87NW	201 87	Fractures are about 5 m long.
N50E / 86SE	50 86	
N15W / 85NE	345 85	Fractures are about 2 m long
N12W / 86NE	348 86	
N10E / 87NW	190 87	
N7E / 86NW	187 86	
N19E / 89NW	199 89	Calcite filled fractures whose apertures are around 0.5 cm.
N11E / 54SE	11 54	
N24E / 89	204 89	
N-S / 86W	0 86	
N7E / 86NW	7 86	
N16W / 86NE	344 86	
N4E / 89 NW	184 89	
N4W / 89NE	356 89	
N11E / 89NW	191 89	
N13E / 89NW	193 89	
N10E / 89NW	190 89	These are general stike and dip for 17 fractures. They have calcite fillings and less than a foot spacing.
N7W / 85NE	353 85	
N3E / 86NW	183 86	
N17E / 88SE	17 88	
N23E / 89NW	203 89	These are general strike and dip for 11 fractures. They have calcite fillings and about half a foot spacing.

N47E / 89NW	227 89	
N9E / 89NW	189 89	
N24E / 87NW	204 87	
N33E / 73NW	213 73	
N5E / 85NW	185 85	
N37E / 89NW	217 89	
N74E / 84NW	254 84	
N56E / 88NW	236 88	20 m to the fault and fractures cut each other. They have calcite fillings with thickness between 0.2-1cm.
N53E / 84NW	233 84	
N15E / 80-85N'	195 83	Calcite filled fractures.
N65E / 68NW	245 68	
N61E / 76NW	241 76	
N81E / 85NW	261 85	
N41E / 86NW	41 86	
N50W / 57NE	310 57	
N10E / 63SE	190 63	
N43E / 69NW	223 69	
N83E / 60NW	263 60	
N70E / 85SE	70 85	
N67E / 87NW	247 87	
N52E / 86NW	232 86	
N47E / 86NW	227 86	
N28E / 84NW	208 84	
N47E / 88NW	227 88	
N50E / 83NW	230 83	
N20E / 44NW	200 44	Calcite filled fractures represents 8 fractures, whose length are bigger than 10 m and have around 0.1 cm aperture.
N27E / 43NW	207 43	
N80W / 85NE	280 85	
N74W / 89 NE	286 89	
N81W / 83NE	279 83	
N55W / 76SW	125 76	
E-W / 81N	270 81	
N37E / 87NW	217 87	Calcite filled fractures.
N53E / 88NW	233 88	
N27E / 77NW	207 77	
N22E / 64NW	202 64	
N85E / 72NW	265 72	Calcite filled fractures.
N82E / 76NW	262 76	
N59E / 54NW	239 54	
N31E / 77NW	211 77	
N33E / 73NW	213 73	
N33E / 79NW	213 79	
N22E / 87NW	202 87	
N18E / 62NW	198 62	

N38E / 71NW	118 71	
N28E / 79NW	208 79	
N26E / 84NW	206 84	It is on the fault zone, calcite filled fractures.
N68E / 55NW	248 55	
N55E / 87NW	235 87	
N26E / 86NW	206 86	
N15E / 81NW	195 81	
N5E / 83NW	185 83	Calcite filled fractures.
N4E / 85NW	184 85	
N11E / 89NW	191 89	
N8E / 89NW	188 89	
N22E / 82NW	202 82	
N-S / 88 W	180 89	Calcite filled fractures.
N3W / 88NE	357 88	
N78E / 87NW	258 89	
N26E / 81NW	206 81	
N15W / 71NE	345 71	
N15W / 72NE	345 72	Open fractures
N21W / 65NE	339 65	
N17W / 84NE	343 84	
N11W / 87NE	349 87	
N-S / 88W	180 88	Calcite filled fractures, 10 m to the fault.
N60E / 63NW	240 63	
N81E / 52NW	261 52	
N80E / 74NW	260 74	
N73E / 72NW	253 72	
N55E / 70NW	235 70	Calcite filled fractures.
N66E / 79NW	246 79	
N30W / 88NE	330 88	
N18W / 79SW	162 79	
N57W / 85NE	303 85	
N60W / 83NE	300 83	
N-S / 66W	180 66	These are general strike and dip for 5 fractures whose spacings are around 3 ft (1 m).
N10E / 67NW	190 67	
N15E / 56NW	195 56	
N70E / 81NW	250 81	Calcite filled fractures.
N79E / 85NW	259 85	
N75E / 83NW	255 83	
N65E / 79NW	245 79	
N70E / 79NW	250 79	
N83E / 81NW	263 81	
N73E / 81NW	253 81	Calcite filled fractures whose apertures are about 0.1mm.
N56E / 56NW	236 56	Calcite filled fractures.
N26E / 41NW	206 41	
N63E / 87NW	243 87	

N47E / 86NW	227 86	Calcite filled fractures
N58W / 86NE	302 86	These are general stike and dip for 4 fractures whose spacing are around 3 ft (1 m). They are filled by calcite.
N45W / 85NE	315 85	
N30W / 87NE	330 87	Open fractures
N70E / 86NW	250 86	These are general strike and dip for 9 calcite filled fractures whose aperture is around 0.1 mm and having less than half a foot spacing.
E-W / 90	90 90	These are general strike and dip for 12 fractures. They have calcite fillings and about half a foot spacing.Their lengths are around 30 m.
N80E / 81NW	260 81	
N41E / 83NW	221 83	
N63E / 66NW	243 66	Calcite filled fractures.
N50E / 65NW	230 65	
N83E / 72NW	263 72	
N84E / 67NW	264 67	Calcite filled fracture.
N85W / 72NE	275 72	
N87E / 85NW	267 85	
N65E / 86NW	245 86	
N87W / 74NE	273 74	Calcite filled fractures.
N81E / 87SE	81 87	
N83W / 71NE	253 71	
N84E / 65NW	264 65	
N63E / 75NW	243 75	Calcite filled fractures.
N71E / 79NW	251 79	
N85W / 73NE	275 73	
N80W / 51NE	280 51	Open fracture.
N81W / 64NE	279 64	
N57E / 80NW	227 80	
N81W / 71NE	279 71	
N39E / 32SE	39 32	
N57E / 71NW	227 71	
N45E / 81NW	225 81	
N78W / 73NE	282 73	
N73W / 69NE	287 69	
N78W / 81NE	282 81	
N55E / 58SE	55 58	
N80W / 41SW	100 41	
N69E / 44SE	69 44	
N37E / 78SE	37 78	Calcite filled fractures.
N45E / 64NW	225 64	
N61E / 79NW	241 79	
N67W / 86NE	337 86	
N42E / 87NW	222 87	
N75W / 73NE	285 73	

N44E / 83NW	224 83	
N43E / 86SE	43 86	Calcite filled fractures, whose lengths are 3m.
N40E / 86SE	40 86	
E-W / 83N	270 83	Calcite filled fractures.
N18E / 73SE	18 73	
N31E / 81SE	31 81	Calcite filled fractures.
N28E / 76SE	28 76	
N56W / 81SW	124 81	
N56W / 80SW	124 80	
N68W / 79SW	112 79	
N54W / 83SW	216 83	Calcite filled fractures.
N28E / 81NW	208 81	
N15E / 81NW	195 81	
N55W / 83SW	125 83	
N60W / 81SW	120 81	
N86W / 83SW	94 83	
N26E / 85NW	206 85	
N26E / 76NW	206 76	
N31E / 76NW	211 76	
N58E / 75SE	58 75	
N19E / 85NW	199 85	
N51E / 88NW	231 88	
N63E / 79SE	63 79	
N27E / 77NW	207 77	
N27E / 86NW	207 86	
E-W / 90	90 90	These are general strike and dip for 5 fractures whose spacing 2, 1 1/2, 1 1/2, 1 1/2. Their aperture is aound 0.5 mm. They are filled by calcite.
N24E / 81NW	204 81	
N25E / 74NW	205 74	Calcite filled fractures.
N16E / 83NW	196 83	

APPENDIX B

Data for Fracture Spacing

SET 1

Scanline No.	Fracture Spacing(ft)
1	1/2, 1, 3/2, 19
2	9
7	1 1/2, 1 1/2, 2 1/2, 1
10	11
12	3
17	2 3/4, 3 3/4, 5 1/2, 4 1/2, 5 3/4
Zone within 40 ft to fault	1, 1/2, 1/2, 1/4, 3/4, 2/3, 1/2, 1/2, 1, 1/2, 1, 1/2

SET 2

Scanline No.	Fracture Spacing(ft)
20	8
Zone within 40 ft to fault	1/2, 1/4, 1/4, 1/4, 1/4, 1/2, 1/2, 1/4

SET 3

Scanline No.	Fracture Spacing(ft)
3	2, 1/2, 1/2, 1
18	8
Zone within 40 ft to fault	1/2, 1/2, 1/2, 1/2, 1/2, 1/2, 1/2, 1/2, 1/2, 1/2

SET 4

Scanline No.	Fracture Spacing(ft)
10	7, 9
14	5 1/2, 9, 2 1/4, 1/2, 1 3/4, 4 1/2, 1/2
Zone within 40 ft to fault	2, 1 1/2, 1 1/2, 1 1/2, 1/2, 1/2, 1/2, 1/2, 1/2, 1/2, 1/2, 1/2, 1/2, 1/4, 1/2

SET 5

Scanline No.	Fracture Spacing(ft)
2	8, 9
7	8, 2 1/2, 2 1/2, 2, 1 1/2
8	3, 7 1/2,
16	5, 2 1/2
Zone within 40 ft to fault	3, 2 1/2, 3, 2 1/2

SET 6

Scanline No.	Fracture Spacing(ft)
4	1/2, 1, 3
9	4, 5
10	5, 7, 5 3/4
11	4 1/2, 3 1/2
13	4 1/4, 3
15	3 3/4, 3, 6 1/2
Zone within 40 ft to fault	3, 3, 3

APPENDIX C

Data for Compartments Area

Box 1		Box 2		Box 3	
Mid points*	**Area (ft2)**	**Mid points***	**Area (ft2)**	**Mid points***	**Area (ft2)**
35	1	550	24	915	445
57	1	544	38	900	890
67	1	545	58	955	1363
86	1	557	65	935	1510
98	1.3	552	77.5	920	1761
64	1.5	498	85	950	1829
52	1.7	485	111	940	1968
51	3	468	118	915	2371
92	3	510	119	905	2662
78	3.3	488	120	1010	2904
76	3.3	477	136	995	2913
62	3.5	455	155	975	3146
52	4	445	160	985	3726
77	4.7	530	169	1035	4414
102	5.3	516	189	1010	5285
74	6	462	225	1065	5924
57	6.3	455	230	1075	6388
68	7	452	258	1030	6680
90	7	577	288	1060	7231
85	7.3	570	311	1060	7356
35	8	587	331	1085	7453
34	8.1	601	360	1075	7667
34	10.1	602	363	1120	8015
33	10.5	555	408	1100	8053
28	11	527	437	1140	8808
37	13	470	456	1155	9583
39	16.3	478	460	1070	10454
46	17.7	600	500	1040	10822
45	17.9	590	600	990	12584
65	20	490	624	955	12584
Mean	6.8		249		5560

* Mid points is the distance from the mid point of each compartment to the Alkali Fault

APPENDIX D

GPS Data for Alkali Fault and Scanline Locations

Alkali Fault Coordinates

Easting	Northing	Elevation	Max_PDOP
295601.600	4916494.290	1903.180	3.0
295587.321	4916492.783	1905.477	7.7
295562.881	4916491.975	1898.520	2.9
295499.899	4916492.555	1893.847	6.9
294722.014	4916475.906	1853.926	2.3
294702.390	4916476.820	1854.174	2.3
294339.385	4916445.985	1814.388	2.9
294326.451	4916446.267	1812.654	3.0
294297.396	4916441.235	1803.915	3.0
294159.591	4916420.438	1797.680	2.3
294187.231	4916422.623	1800.269	2.3
294137.488	4916422.247	1792.977	2.4
294104.411	4916423.021	1789.721	2.4
294081.162	4916424.682	1789.380	2.4
294051.096	4916429.002	1782.669	2.4
293698.250	4916413.953	1744.074	2.8
293685.928	4916419.530	1742.037	2.8
295672.428	4916501.427	1897.315	2.0
295853.431	4916531.965	1888.067	1.9
295868.633	4916538.040	1890.413	1.9
296010.148	4916553.776	1886.540	2.1
296214.782	4916567.029	1888.303	1.7
296289.456	4916593.686	1892.353	2.1
296413.784	4916625.082	1916.529	1.7
296608.095	4916661.758	1928.046	1.7
296630.344	4916674.844	1931.183	2.3
296746.170	4916649.181	1952.463	2.3
297102.647	4916597.522	1955.884	2.9
297141.169	4916605.486	1962.332	2.9
297617.082	4916601.185	1969.691	3.1
297499.735	4916616.968	1956.033	3.2
290915.000	4912823.000		
290915.000	4918569.000		
300840.000	4912823.000		

PDOP (Position Dilution of Precision) is a dimensionless value that is based on the configuration of satellites in the sky. The lower numbers (>4) indicate better satellite configurations which will result in more accurate location determination Higher values (>6) indicate poor satellite geometry that will lead to poor location determination (Ciftci, 2001).

Scanline Coordinates

Scanlines	Easting(X)	Northing(Y)	Elevation
Scanline 1	294118.676	4916347.286	1816.766
Scanline 2	294106.736	4916353.513	1815.719
Scanline 3	295401.277	4916286.234	1866.393
Scanline 4	295398.864	4916287.721	1866.084
Scanline 5	295558.137	4916376.013	1883.006
Scanline 6	295556.748	4916378.373	1883.598
Scanline 7	294927.846	4916399.888	1835.851
Scanline 8	294920.833	4916400.184	1835.012
Scanline 9	295614.099	4915476.536	1785.260
Scanline 10	295614.897	4915484.948	1786.476
Scanline 11	295552.472	4915594.755	1781.919
Scanline 12	295552.867	4915603.443	1778.708
Scanline 13	295521.174	4916403.828	1880.448
Scanline 14	295538.088	4916381.699	1882.989
Scanline 15	295329.011	4916250.747	1834.704
Scanline 16	295413.947	4916357.434	1851.814
Scanline 17	294687.067	4916046.959	1778.556
Scanline 18	297612.934	4916566.754	1966.370
Scanline 19	295329.098	4916250.684	1834.855
Scanline 20	295406.003	4916262.896	1836.874